VECTOR COLOR TRANSPARENCY

W. R. Greenberg* and G. A. Miller

Department of Physics, FM-15

University of Washington, Seattle, WA 98195

Abstract

Color transparency (CT) in high momentum transfer $(e, e'\vec{p})$ reactions is explored. The spin of the proton and photon are treated explicitly, hence the name "Vector CT". The Dirac distorted wave impulse approximation is used as a starting point; then CT effects are embedded. A hadronic basis is used to describe the struck proton as a wavepacket of physical baryon resonances. The effects of the wavepacket expansion on the normal component of the ejectile polarization, which vanishes in the limit of full CT, are investigated. This formalism is also applied to study CT effects in total cross sections, individual separated nuclear response functions, Fermi motion of the initial nucleon, non-zero size of the initial wavepacket and the effects of relativistic lower components. We show that including CT reduces the violations of current conservation (CC), a typical problem in calculations of this kind. The energy dependence of the normal polarization in $(e, e'\vec{p})$ reactions is found to be slow. However, a measurement of the normal transverse response in a heavy nucleus, such as ^{208}Pb seems to afford the opportunity to see CT at quite low momentum transfers. The effects of Fermi motion are investigated, and choosing the momentum of the struck nucleon to be large leads to significant violations of CC.

PACS numbers: 12.38Aw, 13.60-r, 13.85, 24.85.+p

I. INTRODUCTION

Color Transparency (CT) is the postulated [1,2] absence of final- (or initial-) state inter-actions caused by the cancellation of color fields of a system of quarks and gluons with small spatial separation. For example, suppose an electron impinges on a nucleus knocking out a proton at high momentum transfer. The consequence of color transparency is that there is no exponential loss of flux as the ejected particle propagates through the nucleus. Thus, the usually "black" nucleus becomes transparent. We restrict our attention to processes for which the fundamental reaction is elastic, or at least a two-body reaction. This requires that the nuclear excitation energy be known well enough to ensure that no extra pions are created. This subject is under active experimental investigation [3–10].

The existence of color transparency depends on: (1) the formation of a small-sized wave-packet in a high momentum transfer reaction. (2) the interaction between such a small object and nucleons being suppressed (color neutrality or screening) and (3) the wave-packet escaping the nucleus while still small [1,2]. That color neutrality (screening) causes the cross section of small-sized color singlet configurations with hadrons to be small was found in Refs. [11–15], and is well-reviewed in Refs. [16–19]. So we take item (2) as given. The truth of item (1), for experimentally available energies, is an interesting issue. It is discussed in Refs. [19–21], and is not probed in depth here.

It is also true that, for present experiments [3–10], the small object does expand as it moves through the nucleus. Thus the final-state interactions are suppressed but not zero. The importance of this expansion was found by Farrar et al. [22], and by Jennings and Miller [23–26]. See also Refs. [27,28].

Up until now, all calculations of CT have totally neglected the effects of spin. In this paper, the full Lorentz structure of the matrix element for the electroproduction of nucleons from nuclei is considered. We call this work Vector Color Transparency, where the vector moniker derives from the vector nature of the photon exchanged in the hard collision.

What do we hope to gain by introducing this complication? First, experience has shown that the introduction of spin into many physical problems led to totally new phenomena. Whether or not this happens in discussions of CT is the subject of this paper. Second, by invoking time-reversal and parity invariance of the electromagnetic and strong interactions,

the normal component of the polarization of the ejected proton [in $(e, e'\vec{p})$ experiments] must vanish in the limit where final-state interactions are absent [29]. This is the limit of full CT. Therefore, the spin dependent observables provide a very sensitive measure of the effects of CT. Thirdly, we will soon see that the spin dependent observables are defined in terms of ratios of sums of response functions. Thus, experimental measurement of such observables are less susceptible to systematic errors than, for instance, the unpolarized observables. Lastly, an experiment has been proposed and approved, to be run at CEBAF [8], which will measure the energy dependence of the unpolarized cross section and the normal component of the ejected proton's polarization. In that case, it is desirable to have ready theoretical predictions, crude though they might be, to be confronted by the experimental results.

In a previous paper [30] a multiple-scattering series for the color transparency wavepacket-nucleon interaction, within the framework of Glauber (eikonal) theory, was developed. The approach here is the same, except that four-component Dirac spinors are used for both scattered wavefunctions and bound states. As in Ref. [30], we embed CT operators and states into the usual DWBA treatment.

The organization of this paper is as follows. In Section II we display formulae for the $(e, e'\vec{p})$ cross section and polarization in terms of the nuclear response functions, the hadronic tensor, and the nuclear current matrix element (NCME). In Section III the scattering state wavefunction is derived within the context of the Dirac impulse approximation. Most of the material in Sections II and III is well-known, but we present these sections as necessary preliminaries to including the effects of CT. This is done in Section IV, by including the effects of the composite nature of the nucleon. We develop approximation schemes, as in Ref. [30], to evaluate the CT wavefunctions, in Section V. Section VI contains a demonstration that there is at least one reliable approximation scheme for each range of energies. In this section, we also present numerical results for total cross section ratios, integrated longitudinal and transverse nuclear responses, current conservation violations, differential unpolarized cross sections, differential normal polarizations, individual nuclear response functions, effects of non-zero wavepacket size, Fermi motion, and the effects of the purely relativistic lower components of the bound and scattered state wavefunctions. In the final section, Section VII, we summarize and make some concluding comments.

The publication of the results of the SLAC experiment [6] is imminent but not published now. It is important to use the experimental acceptance in computing observables. Thus we leave a detailed assessment of that experiment to a future publication. We also make no attempt to completely review the CT literature.

II. THE NUCLEAR CURRENT MATRIX ELEMENT AND CROSS SECTION

We now describe the spin-dependent formalism. In particular, consider the case of bombarding a spin-0 nucleus with polarized electrons and detecting polarized protons which are knocked out. This process is usually written as $(\vec{e}, e'\vec{p})$. The incoming electron has helicity h and the outgoing nucleon is polarized, in its rest frame, along $\check{s}_R$. A schematic drawing of the $(\vec{e}, e'\vec{p})$ reaction is shown in Figure 1. The following discussion reproduces the essential points of Ref. [31]

The kinematical situation is shown in Figure 2. We take the virtual photon to lie along the $\check{Z}$ direction, and the electron scattering plane to be the YZ plane. The scattering amplitude for Vector CT is defined as

$$M_\alpha = j_\mu J_\alpha^\mu, \tag{2.1}$$

where j_μ is the matrix element of the electron current and J_α^μ is the matrix element of the nuclear current (NCME). In the one-photon exchange approximation and using the nuclear shell model, the cross section is

$$\frac{d^3\sigma}{d\epsilon_{k'} d\Omega_{k'} d\Omega_p} = \frac{M_N |\mathbf{p}|}{(2\pi)^3} \left(\frac{d\sigma}{d\Omega_{k'}} \right)_{Mott}$$
$$\times \quad \sum_\alpha \int dE_p |M_\alpha|^2 \delta(E_p - q^0 - M_N + \varepsilon_\alpha), \tag{2.2}$$

where $k^\mu(k'^\mu)$ is the four-momentum of the incoming (outgoing) electron, $q^\mu = k^\mu - k'^\mu$. The binding energy of the nucleon in shell α is ε_α. This is small compared with other energy scales in the problem and is neglected. The sum is over all occupied shells. The four-momentum of the outgoing nucleon is p^μ and its energy is denoted by $p^0 = E_p$; M_N is the nucleon mass. The solid angle $d\Omega_p = \sin \zeta \, d\zeta \, d\beta$. The nucleus is assumed to recoil with negligible energy. The Mott cross section is defined in Ref. [31]

4

The square of the matrix element M_α can be written in terms of electron and nuclear tensors:

$$|M_\alpha|^2 = \eta_{\mu\nu} W_\alpha^{\mu\nu}, \tag{2.3}$$

The electron tensor $\eta_{\mu\nu} = \frac{1}{2}\left(k_\mu k'_\nu + k_\nu k'_\mu - g_{\mu\nu} k \cdot k' + ih\epsilon_{\mu\nu\lambda\kappa} k'^\lambda k^\kappa\right)$, where $g_{\mu\nu}$ is the metric tensor with $g_{00} = -g_{11} = -g_{22} = -g_{33} = 1$, and $\epsilon_{\mu\nu\alpha\beta}$ is the completely antisymmetric fourth rank tensor. The electron helicity is given by h. Here and throughout we use the notation and conventions of Bjorken and Drell [32].

We turn now to the nuclear tensor. This depends on the direction of the (rest-frame) spin of the ejected proton. Thus, $W_\alpha^{\mu\nu} = W_\alpha^{\mu\nu}(\check{\mathbf{s}}_R)$ where we use the notation that $\check{\mathbf{a}}$ describes a unit vector in the direction of $\mathbf{a}$. The upside-down "hat" is used to distinguish unit vectors from operators. The nuclear tensor is

$$W_\alpha^{\mu\nu}(\check{\mathbf{s}}_R) = J_\alpha^{\mu*}(q) J_\alpha^\nu(q), \tag{2.4}$$

where $J_\alpha^\nu(q)$ are the matrix elements of the nuclear electromagnetic current operator. All of the unknown physics is lumped into the nuclear current. Therefore, we define the quantity,

$$\overline{W}^{\mu\nu}(\check{\mathbf{s}}_R) = \sum_\alpha \int dE_p\, W_\alpha^{\mu\nu}(\check{\mathbf{s}}_R)\, \delta\left(E_p - q^0 - M_N + \varepsilon_\alpha\right), \tag{2.5}$$

where the sum is over all occupied single-particle shells and the integral and delta function serve to conserve energy in this full nuclear tensor. The nuclear tensor $W_\alpha^{\mu\nu}$ depends on the ejected proton energy, E_p, because the scattered proton is ultimately detected, on the mass shell, moving with momentum $\mathbf{p}$.

Thus, the crucial quantity is the nuclear current matrix element (NCME). We now present a symbolic form for this current. The NCME is given by

$$J_\alpha^\mu(q) = {}^{(-)}\langle\Psi_{\mathbf{p},\check{\mathbf{s}}_R}|T_H^\mu(q)|\alpha\rangle. \tag{2.6}$$

where the initial state of this knockout process is labelled by the shell model state of a bound proton, α. In the final state, a proton moves with a momentum $\mathbf{p}$ with some rest frame spin $\check{\mathbf{s}}_R$. The residual nucleus is an α-hole state, which is not detected and is therefore summed over. The initial and final states are connected by a vector operator denoted as $T_H^\mu(q)$ which describes the absorption of a virtual photon on a proton in the nucleus. The overlap of the

5

initial and final nuclear states is imagined to be a single particle state of a nucleon bound in shell model state α. Incoming boundary conditions for the proton scattered wave are used, but we can also use outgoing boundary conditions:

$$J_\alpha^\mu(q) = \langle\alpha|T_H^{\mu\dagger}(q)|\Psi_{\mathbf{p},-\check{\mathbf{s}}_R}\rangle^{(+)}. \tag{2.7}$$

A more complete derivation is described elsewhere [31].

We contract the indices of the electron and nuclear tensors to obtain the differential cross section. The use of current conservation: $q_\mu J^\mu = q^0 J^0 - q^3 J^3 = 0$, where $\mathbf{q} \equiv q^3\check{\mathbf{Z}}$ allows us to eliminate the longitudinal components of the nuclear current in favor of the better known charge density. In particular, $W^{33} = \frac{q_0^2}{q_3^2}W^{00}$ and $W^{3k} = \frac{q_0}{q_3}W^{0k}$ for $k \neq 3$. We note here an important point concerning current conservation and gauge invariance. The NCME is an integral over a bound state wavefunction, a scattered state wavefunction and an operator which connects the two. If these two wavefunctions are derived from the same theory, as they are in nature, then as members of a complete set they are orthogonal and current is conserved. If the bound and scattered states are modelled with different Hamiltonia, as usually practiced, there is no guarantee that the wavefunctions are orthogonal and that current is conserved. This problem is discussed in Section V where we show that current is conserved in our calculation at the $< 10\%$ level or better.

The above discussion leads to the differential cross section for the scattering of polarized electrons (helicity h) off of a nucleus, ejecting a proton with rest- frame spin $\check{\mathbf{s}}_R$ [31]:

$$\sigma_h(\check{\mathbf{s}}_R) \equiv \left(\frac{d^3\sigma}{d\epsilon_{k'}d\Omega_{k'}d\Omega_p}\right)_{h,\check{\mathbf{s}}_R} \tag{2.8}$$

$$= \frac{M_N|\mathbf{p}|}{2(2\pi)^3}\left(\frac{d\sigma}{d\Omega_{k'}}\right)_{Mott}\left\{V_L\left(R_L + R_L^n\mathcal{S}_n\right) + V_T\left(R_T + R_T^n\mathcal{S}_n\right)\right.$$
$$+V_{TT}[(R_{TT} + R_{TT}^n\mathcal{S}_n)\cos 2\beta + \left(R_{TT}^t\mathcal{S}_t + R_{TT}^l\mathcal{S}_l\right)\sin 2\beta]$$
$$+V_{LT}[(R_{LT} + R_{LT}^n\mathcal{S}_n)\sin\beta + \left(R_{LT}^t\mathcal{S}_t + R_{LT}^l\mathcal{S}_l\right)\cos\beta]$$
$$+hV_{LT}'[(R_{LT}' + R_{LT}'^n\mathcal{S}_n)\cos\beta + \left(R_{LT}'^t\mathcal{S}_t + R_{LT}'^l\mathcal{S}_l\right)\sin\beta]$$
$$\left.+hV_{TT}'\left(R_{TT}'^t\mathcal{S}_t + R_{TT}'^l\mathcal{S}_l\right)\right\}, \tag{2.9}$$

where kinematical factors V are defined by $V_L = \left(\frac{q^2}{|\mathbf{q}|^2}\right)^2$, $V_T = \tan^2\frac{\theta_e}{2} - \frac{q^2}{2|\mathbf{q}|^2}$, $V_{TT} = -\frac{q^2}{2|\mathbf{q}|^2}$, $V_{LT} = \frac{q^2}{|\mathbf{q}|^2}\left(\tan^2\frac{\theta_e}{2} - \frac{q^2}{|\mathbf{q}|^2}\right)^{1/2}$, $V_{LT}' = \frac{q^2}{|\mathbf{q}|^2}\tan\frac{\theta_e}{2}$, $V_{TT}' = \tan\frac{\theta_e}{2}\left(\tan^2\frac{\theta_e}{2} - \frac{q^2}{|\mathbf{q}|^2}\right)^{1/2}$, where θ_e

is the electron scattering angle, $q^2 = q_\mu q^\mu$, and $|\mathbf{q}|$ is the magnitude of the photon three-momentum. The direction of the ejected proton's spin is given, in its rest frame, by $\check{\mathbf{s}}_R$. The spin projections which appear in the above cross section are identified to be: $\mathcal{S}_n = \check{\mathbf{n}} \cdot \check{\mathbf{s}}_R$, $\mathcal{S}_l = \check{\mathbf{l}} \cdot \check{\mathbf{s}}_R$, $\mathcal{S}_t = \check{\mathbf{t}} \cdot \check{\mathbf{s}}_R$, where the unit vectors are $\check{\mathbf{n}} = \check{\boldsymbol{\beta}} = (\mathbf{q} \times \mathbf{p})/|\mathbf{q} \times \mathbf{p}|$, $\check{\mathbf{l}} = \check{\mathbf{p}}$ and $\check{\mathbf{t}} = \check{\boldsymbol{\zeta}} = \check{\mathbf{n}} \times \check{\mathbf{l}}$. The quantities R are called the response functions. The subscripts L and T are the contributions from longitudinal and transverse photons (both helicities), respectively. The subscripts TT and LT refer to the transverse- transverse and longitudinal-transverse response of the system. These arise from the interference between the different polarizations of the photon. The subscripts TT' and LT' also arise from the interference of the longitudinal and transverse photons. They are "primed" because they are formed from an antisymmetric combination of components of the nuclear tensor and thus only accessible with a polarized electron beam. The response functions themselves are defined in terms of the hadronic tensor. Explicitly,

$$\frac{1}{2}\left(R_L + R_L^n \mathcal{S}_n\right) = \overline{W}^{00}(\check{\mathbf{s}}_R), \tag{2.10}$$

$$\frac{1}{2}\left(R_T + R_T^n \mathcal{S}_n\right) = \overline{W}^{11}(\check{\mathbf{s}}_R) + \overline{W}^{22}(\check{\mathbf{s}}_R), \tag{2.11}$$

$$\frac{1}{2}[(R_{TT} + R_{TT}^n \mathcal{S}_n)\cos 2\beta + \left(R_{TT}^t \mathcal{S}_t + R_{TT}^l \mathcal{S}_l\right)\sin 2\beta] = \overline{W}^{22}(\check{\mathbf{s}}_R) - \overline{W}^{11}(\check{\mathbf{s}}_R), \tag{2.12}$$

$$\frac{1}{2}[(R_{LT} + R_{LT}^n \mathcal{S}_n)\sin \beta + \left(R_{LT}^t \mathcal{S}_t + R_{LT}^l \mathcal{S}_l\right)\cos \beta] = \overline{W}^{02}(\check{\mathbf{s}}_R) + \overline{W}^{20}(\check{\mathbf{s}}_R), \tag{2.13}$$

$$\frac{1}{2}[(R_{LT}' + R_{LT}'^n \mathcal{S}_n)\cos \beta + \left(R_{LT}'^t \mathcal{S}_t + R_{LT}'^l \mathcal{S}_l\right)\sin \beta] = i\left[\overline{W}^{10}(\check{\mathbf{s}}_R) - \overline{W}^{01}(\check{\mathbf{s}}_R)\right], \tag{2.14}$$

$$\frac{1}{2}[\left(R_{TT}'^t \mathcal{S}_t + R_{TT}'^l \mathcal{S}_l\right)] = i\left[\overline{W}^{12}(\check{\mathbf{s}}_R) - \overline{W}^{21}(\check{\mathbf{s}}_R)\right]. \tag{2.15}$$

Since the response functions, as defined above, are independent of β, certain restrictions can be imposed using simple kinematical arguments. In particular, in "parallel kinematics" when $\vec{p} = \vec{q}$, all of the response functions must vanish except for R_L, R_T and $R_{TT}'^l$, which are unconstrained, and the normal and transverse parts of R_{LT} and R_{LT}' which are constrained to be opposites [31,33]. We point out that the constraints of parallel kinematics have been

violated in the work of Allder [34]. Refs. [31] and [33] show how these response functions can be extracted from the cross section.

Now, we leave the general theory of the $(\vec{e}, e'\vec{p})$ reaction and focus on the upcoming CEBAF experiment [8]. Saha and collaborators plan on measuring the unpolarized cross section and the normal component (to the photonuclear scattering plane) of the proton polarization. In terms of the above notation, the unpolarized differential cross section is [35]

$$
\sigma_0(0) = \frac{M_N|\mathbf{p}|}{(2\pi)^3} \left(\frac{d\sigma}{d\Omega_{k'}}\right)_{Mott} \{V_L R_L + V_T R_T \\
+ V_{TT} R_{TT} \cos 2\beta + V_{LT} R_{LT} \sin\beta\}, \tag{2.16}
$$

where the subscript 0 on σ signifies that electron helicity is averaged and the argument of 0 implies that the direction of the ejected proton spin is averaged over. The normal component of the polarization vector is then defined as

$$
P_n^0 = \frac{1}{\sigma_0(0)} \frac{M_N|\mathbf{p}|}{(2\pi)^3} \left(\frac{d\sigma}{d\Omega_{k'}}\right)_{Mott} \{V_L R_L^n + V_T R_T^n \\
+ V_{TT} R_{TT}^n \cos 2\beta + V_{LT} R_{LT}^n \sin\beta\}. \tag{2.17}
$$

Since the normal component of the polarization, P_n^0, is dependent only on normal response functions which vanish in the high energy of the CT limit, P_n^0 also vanishes in that limit. Parity and time reversal invariance imply that non-zero values of P_n^0 arise only from the final-state spin-orbit interaction. If CT is obtained *all* final-state interactions vanish, so that P_n^0 vanishes too.

It is also useful to consider the "total" unpolarized cross section, obtained by integrating over the solid angle of the outgoing proton. If we integrate over β in Eq. (2.16), all of the terms which have explicit β dependence vanish. It then remains to integrate over $\sin\zeta\, d\zeta$. However, at this stage, we introduce the convenient approximation that $d\Omega_p \approx d^2|\mathbf{p}-\mathbf{q}|/|\mathbf{q}|^2$. Since the response functions are functions only of $\mathbf{q}_\perp \equiv \mathbf{p} - \mathbf{q}$, $(q_\perp = |\mathbf{q}_\perp|)$ we define the total unpolarized cross section as

$$
\sigma \equiv \frac{d^2\sigma}{d\epsilon_{k'} d\Omega_{k'}} \tag{2.18}
$$

$$
= \frac{M_N|\mathbf{p}|}{(2\pi)^2 |\mathbf{q}|^2} \left(\frac{d\sigma}{d\Omega_{k'}}\right)_{Mott} \\
\times \int dq_\perp\, q_\perp \{V_L R_L(q_\perp) + V_T R_T(q_\perp)\}. \tag{2.19}
$$

8

The above equations completely specify the relationship between the response functions of the $(e, e'\vec{p})$ reaction and the experimental observables which will be measured in the near future. The crucial quantity is the electromagnetic nuclear current matrix element (NCME) of Eq. (2.6).

III. DWBA FORMALISM

A. Bound State

We now discuss the model bound state used here. In Ref. [30], the ejected proton was taken to lie initially in a non-relativistic one-particle harmonic oscillator shell-model state. Since the present formalism is spin dependent and relativistic, it is necessary to look for a relativistic single-particle shell-model state which is a four-component Dirac spinor. There are several such models [36,37]. Here we use the finite nuclei model of Horowitz and Serot [38]. Our opinion is that QHD is not a fundamental field theory. However, for our purposes it is not necessary to consider QHD to be anything but a model, which accounts for nuclear phenomenology. In particular, QHD yields realistic nuclear densities and four-component bound state wavefunctions.

It is useful to display the solution to the Dirac equation of QHD in terms of radial and angular solutions. The set of quantum numbers $\alpha = \{n, j, l, m, t\}$ where n is the principal quantum number, j is the total angular momentum, l is the orbital angular momentum, m is the $\check{\mathbf{Z}}$ component of the total angular momentum and t is the third component of the isospin. Then, the solution is

$$
\begin{aligned}
\langle \mathbf{R} | \alpha \rangle &\equiv \Phi_\alpha(\mathbf{R}) \\
&= \frac{1}{R} \begin{pmatrix} iG_{njl}(R) \\ +F_{njl}(R)\boldsymbol{\sigma} \cdot \check{\mathbf{R}} \end{pmatrix} \mathcal{Y}_{jlm}(\check{\mathbf{R}})\, \eta_t,
\end{aligned} \tag{3.1}
$$

where G and F are functions of the radial variable $R = |\mathbf{R}|$ only and η_t is a two-component isospinor, with $\eta_t = \frac{1}{2}$ for protons and $\eta_t = -\frac{1}{2}$ for neutrons. The quantities $\mathcal{Y}_{jlm}$ are the standard spin spherical harmonics. We use a computer program by Horowitz [39] to generate these radial wavefunctions. Note also that $\Phi_\alpha(\mathbf{R})$ are normalized to unity.

B. Current Operator

The vector current operator represents the absorption of a virtual photon by a nucleon bound in a nucleus. This nucleon is somewhat off the energy shell. In general the current operator can be expressed in terms of scalar functions of the four-momenta multiplied by any of *twelve* four-vectors [33]! Since the bound nucleon is only slightly off shell (the binding energy is small), and since any other choice for this operator is only a guess, the current operator is chosen to be the free nucleon current operator. Thus, we define the configuration-space matrix elements, which are matrices in the Dirac space, as,

$$\langle \mathbf{R}|T_H^\mu(q)|\mathbf{R}'\rangle = e^{i\mathbf{q}\cdot\mathbf{R}}\delta^3(\mathbf{R}-\mathbf{R}')\,\gamma^0\Gamma^\mu(q), \tag{3.2}$$

where

$$\Gamma^\mu(q) = F_1(q^2)\gamma^\mu + \frac{i}{2M_N}F_2(q^2)\sigma^{\mu\nu}q_\nu, \tag{3.3}$$

and $F_1(q^2)$ and $F_2(q^2)$ are the usual Dirac and Pauli form factors of the nucleon. We use a simple dipole parameterization such that

$$G_E(q^2) = \left(1 - \frac{q^2}{0.71\,GeV^2}\right)^{-2}, \tag{3.4}$$

$$G_M(q^2) = (1+\kappa)G_E(q^2), \tag{3.5}$$

where $\kappa = 1.79$ is the anomalous magnetic moment of the proton. The Dirac and Pauli form factors are given by

$$F_1(q^2) = \frac{q^2G_M(q^2) - 4M_N^2G_E(q^2)}{q^2 - 4M_N^2}, \tag{3.6}$$

$$F_2(q^2) = \frac{4M_N^2}{q^2 - 4M_N^2}\left[G_E(q^2) - G_M(q^2)\right]. \tag{3.7}$$

This assumption of the current operator neglects the possibility that the nucleon properties are much modified in medium.

C. Optical Potential and Distorted Wave

We now describe the wavefunction of the scattered proton. Here the bound state proton wavefunction is a relativistic four-component object, and the current operator is a 4 × 4

matrix. Thus the proton wave must also be a Dirac spinor, satisfying a one-particle Dirac equation.

Treating the Dirac equation as a one-particle equation has many serious diseases. Indeed, problems of interpretation with the negative energy states led to the development of quantum field theory. However, the difficulties can be identified (see e.g. Section 2 of Ref. [40].) Here we are interested in the scattering of energy eigenstates of an interacting Dirac Hamiltonian. Such eigenstates propagate along with no transitions to the negative energy states. In these situations, there is no problem in the interpretation of the Dirac equation as the governing equation of a single particle relativistic quantum mechanics.

In the early eighties, a phenomenology based on using the Dirac equation to describe the scattering of medium energy protons from nuclei was developed. Both partial wave analyses [41,42] and eikonal reductions of the Dirac equation [43–46] have been performed. The successes of these models, most notably the spin observables such as analyzing powers and spin rotation functions, as well as differential cross sections, are still quite impressive. From the standpoint of CT, where we are interested in very high energy scattering, the eikonal form is appropriate.

Let us now discuss the potentials that enter into the Dirac equation. In the impulse approximation these are complex Lorentz scalars and time-components of 4-vectors. We label these V_s and V_v, respectively. In the relativistic impulse approximation, the scalar and vector optical potentials, V_s and V_v, are proportional to forward Dirac scalar and Dirac vector scattering amplitudes (F_s^0, F_v^0) and to the scalar and vector nuclear densities [47–53] (ρ_s, ρ_v), such that

$$U_{opt}(\mathbf{R}) = V_s(\mathbf{R}) + \gamma^0 V_v(\mathbf{R}), \tag{3.8}$$

where

$$V_s(\mathbf{R}) = r\, F_s^0 \rho_s(\mathbf{R}) \quad \text{and} \quad V_v(\mathbf{R}) = r\, F_v^0 \rho_v(\mathbf{R}), \tag{3.9}$$

and $r = -4\pi i p_{lab}/M_N$ is a kinematical factor needed to relate the invariant Feynman amplitude to the usual description of the optical potential in the impulse approximation. The scalar and vector nuclear densities are taken from the QHD model in the previous section [38],

11

$$\rho_s(R) = \sum_\alpha \left(\frac{2j_\alpha + 1}{4\pi R^2}\right)\left(|G_\alpha(R)|^2 - |F_\alpha(R)|^2\right), \tag{3.10}$$

$$\rho_v(R) = \sum_\alpha \left(\frac{2j_\alpha + 1}{4\pi R^2}\right)\left(|G_\alpha(R)|^2 + |F_\alpha(R)|^2\right). \tag{3.11}$$

The potential strengths, F_s^0 and F_v^0 are taken directly from NN scattering data [50,54–61]; see Appendix A. Since the strengths are a sensitive function of energy and NN scattering data, we consider our calculations reliable only at the energies where sufficient data exists to determine the strengths F_s^0 and F_v^0.

The Dirac equation for the distorted wave is given by

$$\begin{aligned} H\Psi_{\mathbf{p},\check{s}_R}^{(+)}(\mathbf{R}) = \Big[-i\boldsymbol{\alpha}\cdot\boldsymbol{\nabla} + \beta\left(M_N + V_s(R)\right) \\ + V_v(R)\Big]\Psi_{\mathbf{p},\check{s}_R}^{(+)}(\mathbf{R}) \\ = E\Psi_{\mathbf{p},\check{s}_R}^{(+)}(\mathbf{R}), \end{aligned} \tag{3.12}$$

where $E = \sqrt{p^2 + M_N^2}$. This equation is solved by separation into two coupled first-order differential equations. The eikonal form of the solution to this equation is well known [43–46] and is given by

$$\begin{aligned} \Psi_{\mathbf{p},-\check{s}_R}^{(+)}(\mathbf{R}) = \mathcal{N}\begin{pmatrix} 1 \\ \frac{-i\boldsymbol{\sigma}\cdot\boldsymbol{\nabla}}{E+M_N+V_s(R)-V_v(R)} \end{pmatrix} e^{ipZ} \\ \times \exp\left[\int_{-\infty}^{Z} dZ'\Omega(\mathbf{B}, Z')\right]\chi_{-\check{s}_R}, \end{aligned} \tag{3.13}$$

where $\mathbf{R} \equiv \mathbf{B} + Z\check{\mathbf{Z}}$,

$$\begin{aligned} \Omega(\mathbf{B}, Z') = \frac{1}{2ip}\Big\{U_c(\mathbf{B}, Z') \\ + U_{so}(\mathbf{B}, Z')\left[\boldsymbol{\sigma}\cdot\mathbf{B}\times\mathbf{p} - ipZ'\right]\Big\}, \end{aligned} \tag{3.14}$$

$\mathbf{R}\cdot\mathbf{p} = pZ$, and $\mathbf{B}\cdot\mathbf{p} = 0$. Also note that we have used outgoing boundary conditions and changed the sign of the rest-frame spin projection, as in Eq. (2.7). The normalization is $\mathcal{N} = \sqrt{(E + M_N)/(2M_N)}$. The Dirac scalar and vector potentials have been eliminated in favor of new central (U_c) and spin-orbit (U_{so}) potentials:

$$\begin{aligned} U_c(R) = 2EV_v(R) + 2M_NV_s(R) \\ + V_s^2(R) - V_v^2(R), \end{aligned} \tag{3.15}$$

$$U_{so}(R) = \frac{1}{E + M_N + V_s(R) - V_v(R)}$$
$$\times \frac{1}{R} \frac{\partial}{\partial R} \left\{ V_v(R) - V_s(R) \right\}. \tag{3.16}$$

Note that the potentials U_c and U_{so} have units of $(Energy)^2$; we use the symbol U (and not V) to indicate this. The expression in Eq. (3.13) can be simplified; the detailed form of the wavefunctions is relegated to Appendix B.

Finally, we note one other complication. The eikonal wavefunctions presented in Appendix B have been derived in the limit where the particle travels along the $\check{\mathbf{Z}}$ axis (direction of the virtual photon). At very high energies, the difference between $\check{\mathbf{p}}$ and $\check{\mathbf{Z}}$ is small. Näively, this finite scattering angle should make little difference. However, if one assumes that the scattering angle is exactly zero, then the response function R_{TT} is also exactly zero. Since, in the plane-wave limit, we know this is not true, account must be taken of this scattering angle. We have derived the cross section in Eq. (2.9) with the coordinates that the final proton momentum makes an angle ζ with the $\check{\mathbf{Z}}$-axis (the direction of $\mathbf{q}$) and an angle β with normal to the electron scattering plane (the XZ plane). Call this the q-basis. The derivation of the eikonal wavefunction described above has the proton momentum $\mathbf{p}$ along $\check{\mathbf{Z}}$; call this the p-basis. To move our eikonal wavefunctions from the p-basis to the q-basis, we perform a passive rotation of the coordinates to the desired frame.

IV. INCLUSION OF CT

To include the effects of color transparency, we proceed as in Ref. [30] and include the baryonic internal degrees of freedom. Thus, the states in the full Hilbert space now carry two labels: one for the "external" nuclear space and one for the internal quark space. The quark space operators are identified wearing "hats" and we write CT quantities using script lettering, where possible. Then, the CT scattering matrix element is given by

$$\mathcal{M}_\alpha = j_\mu \mathcal{J}_\alpha^\mu \tag{4.1}$$

where the electron current is j_μ. The triple differential cross section is given by Eq. (2.2), except for the replacement of M_α by $\mathcal{M}_\alpha$. Thus, in order to completely specify the method

for the inclusion of CT effects, it remains to construct the CT generalized NCME. We follow the method in Ref. [30] and write

$$\mathcal{J}_\alpha^\mu(q) = \langle N, \alpha | \widehat{T}_H^{\mu\dagger}(q) | \Psi_{N,\mathbf{p},-\check{s}_R} \rangle^{(+)}, \tag{4.2}$$

Here, $|\Psi_{N,\mathbf{p},-\check{s}_R}\rangle^{(+)}$ is a vector in both internal and external spaces. The subscript on Ψ is to indicate that ultimately a nucleon N moving with momentum $\mathbf{p}$ and rest-frame spin projection $-\check{s}_R$ is detected. The overlap of this state with the nuclear position state $\langle \mathbf{R} |$ gives a vector in the internal space only, which we identify with bold face type: $\langle \mathbf{R} | \Psi_{N,\mathbf{p},-\check{s}_R} \rangle^{(+)} = \mathbf{\Psi}_{N,\mathbf{p},-\check{s}_R}^{(+)}(\mathbf{R})$. The asymptotic boundary condition is implemented by imagining that $\mathbf{\Psi}_{N,\mathbf{p},-\check{s}_R}$ is some internal space vector, whose equation of motion we shall derive below, projected onto the nucleon state $|N\rangle$.

In our approach the relativistic bound state is not changed by including CT effects. See, however, Ref. [62]. The rest of this Section describes the other elements in Eq. (4.2).

A. Current Operator

Upon absorption of a high-energy photon, the proton is converted into a coherent superposition of baryon states (a wavepacket), with components labelled by a discrete quantum number, m. Then, we identify the relevant inelastic transition Dirac and Pauli form factors by taking the matrix elements of the current operator to be

$$\langle N, \mathbf{R} | \widehat{T}_H^\mu(q) | m, \mathbf{R}' \rangle = e^{i\mathbf{q}\cdot\mathbf{R}} \delta^3(\mathbf{R} - \mathbf{R}') \gamma^0 \Gamma_{N,m}^\mu(q), \tag{4.3}$$

where

$$\Gamma_{N,m}^\mu(q) = F_{1_{N,m}}(q^2)\gamma^\mu + \frac{i}{2M_N} F_{2_{N,m}}(q^2)\sigma^{\mu\nu}q_\nu. \tag{4.4}$$

B. Optical Potential

We now consider the optical potentials $V_s(R)$ and $V_v(R)$ to be operators in the internal quark space. These optical potentials are essentially products of the baryon-nucleon scattering amplitude operator $\widehat{f}(\widehat{b}^2)$ with ρ_s or ρ_v. We choose the scalar and vector potentials

14

to have the same operator structure, to be proportional to the same function $f(\widehat{b}^2)$. At present, there is no detailed knowledge about the precise form for $f(\widehat{b}^2)$. However, some general properties are known. For small wavepackets with $b^2 \ll b_H^2$ with $b_H^2 \equiv \langle N|\widehat{b}^2|N\rangle$, f should vanish. Interactions do occur for larger wavepackets. For non-zero but still small sized wavepackets, the interaction goes like

$$\lim_{\widehat{b}^2 \to 0} f(\widehat{b}^2) \to \frac{\widehat{b}^2}{b_H^2}. \tag{4.5}$$

The operator f is normalized such that

$$f(\widehat{b}^2 = 0) = 0, \tag{4.6}$$

$$\langle N|f(\widehat{b}^2)|N\rangle = 1. \tag{4.7}$$

We use a general function $f(\widehat{b}^2)$, subject only to the constraints of Eqs. (4.5)-(4.7). The matrix elements of the scalar and vector operators can then be written as

$$\langle m, \mathbf{R}|\widehat{V}_{s(v)}|m', \mathbf{R}'\rangle = \delta^3(\mathbf{R} - \mathbf{R}')V_{s(v)}(\mathbf{R})\langle m|f(\widehat{b}^2)|m'\rangle. \tag{4.8}$$

To compactify the notation, we define the quantity $V_{s(v)}(\mathbf{R})f(\widehat{b}^2) \equiv \widehat{V}_{s(v)}(\mathbf{R})$.

C. Distorted Wave

In this section we obtain the wave equation for the propagation of the wavepacket formed in the hard collision through the nucleus. Start by considering the time-independent Dirac equation. The equivalent Dirac Hamiltonian should now be considered an operator in the internal quark space. As such, we award H a "hat". All of the tools have already been developed and we immediately write

$$\widehat{H}\mathbf{\Psi}_{N,\mathbf{p},\check{\mathbf{s}}_R}^{(+)}(\mathbf{R}) = \left[-i\boldsymbol{\alpha} \cdot \boldsymbol{\nabla} + \beta\left(\widehat{M} + \widehat{V}_s(R)\right)\right.$$
$$\left. + \widehat{V}_v(R)\right]\mathbf{\Psi}_{N,\mathbf{p},\check{\mathbf{s}}_R}^{(+)}(\mathbf{R})$$
$$= E\mathbf{\Psi}_{N,\mathbf{p},\check{\mathbf{s}}_R}^{(+)}(\mathbf{R}), \tag{4.9}$$

where E is the energy and we have already taken the matrix element in the external configuration space. That is, $\mathbf{\Psi}_{N,\mathbf{p},\check{\mathbf{s}}_R}^{(+)}(\mathbf{R}) = \langle \mathbf{R}|\Psi_{N,\mathbf{p},\check{\mathbf{s}}_R}\rangle^{(+)}$. In this notation, $\widehat{M}^2$ is the baryon

15

mass operator squared. That is, $\widehat{M}^2|m\rangle = M_m^2|m\rangle$; the nucleon is the ground state with $m = N$ having eigenvalue M_N^2. The combination

$$\widehat{\mathbf{p}}^2 \equiv E^2 - \widehat{M}^2 \tag{4.10}$$

is also a quark space operator which can be interpreted as the baryon momentum operator squared. This operator accounts for the different kinematics with which the wavepacket components propagate through the nucleus. Here $\widehat{\mathbf{p}}$ is also a three-vector in the $\check{\mathbf{Z}}$ direction; $\widehat{\mathbf{p}} = \widehat{p}\check{\mathbf{Z}}$.

The Dirac equation can again be solved by eliminating the lower components. Then we see that the CT scalar and vector Dirac potentials (which are operators in the internal space) can be eliminated in favor of combinations given by

$$\widehat{U}_c(R) = 2E\widehat{V}_v(R) + \left\{\widehat{M}, \widehat{V}_s(R)\right\} + \left[\widehat{M}, \widehat{V}_v(R)\right]$$
$$+ \widehat{V}_s^2(R) - \widehat{V}_v^2(R), \tag{4.11}$$

$$\widehat{U}_{so}(R) = \frac{1}{R}\left[\frac{\partial}{\partial R}\left(\widehat{V}_v(R) - \widehat{V}_s(R)\right)\right]$$
$$\times \left(E + \widehat{M} + \widehat{V}_s(R) - \widehat{V}_v(R)\right)^{-1}, \tag{4.12}$$

where the square (curly) brackets are the (anti-) commutator symbols. We also define "path-evolved" versions of the operators of Eqs. (4.11) and (4.12) as

$$\widehat{\mathcal{U}}_{c(so)}(\mathbf{R}) = e^{-i\widehat{p}Z}\frac{1}{\widehat{p}}\widehat{U}_{c(so)}(R)e^{i\widehat{p}Z}. \tag{4.13}$$

Eikonalizing in the usual way, we see that the solution to the resulting eikonal first-order equation is a path-ordered exponential. The notation is simplified by defining an operator $\widehat{\Omega}$ such that

$$\widehat{\Omega}(\mathbf{B}, Z') = \frac{1}{2i}\left[\widehat{\mathcal{U}}_c(\mathbf{B}, Z')\right.$$
$$\left. + \widehat{\mathcal{U}}_{so}(\mathbf{B}, Z')\left(\boldsymbol{\sigma}\cdot\mathbf{B}\times\widehat{\mathbf{p}} - i\widehat{p}Z'\right)\right]. \tag{4.14}$$

Note that $\left[\widehat{\Omega}(\mathbf{R}), \widehat{\Omega}(\mathbf{R}')\right] \neq 0$ since $\widehat{p}$ and $\widehat{b}$ do not commute. This is because $\widehat{p}$ contains $\widehat{M}^2$, and $\left[\widehat{M}^2, f(\widehat{b}^2)\right] \neq 0$.

We want to identify the equivalent CT wavefunctions which are obtained when the NCME is written as

$$\mathcal{J}^{\mu}_{\alpha}(q) = \int d^3R\, \overline{\Phi}_{\alpha}(\mathbf{R})\, e^{-i\mathbf{q}\cdot\mathbf{R}}\, \overline{\Gamma}^{\mu}(q)\, \Psi^{(+)}_{CT,\mathbf{p},-\check{\mathbf{s}}_R}(\mathbf{R}). \tag{4.15}$$

where $\overline{\Phi}_{\alpha}(\mathbf{R}) = \Phi^{\dagger}_{\alpha}(\mathbf{R})\gamma^0$ and $\overline{\Gamma}^{\mu} = \gamma^0\,[\Gamma^{\mu}]^{\dagger}\,\gamma^0$. The bound state, $\Phi_{\alpha}(\mathbf{R})$, is given in Eq. (3.1) and the nucleon current operator is defined in Eq. (3.2). Quite generally, then, the CT wavefunction is given by

$$\Psi^{(+)}_{CT,\mathbf{p},-\check{\mathbf{s}}_R}(\mathbf{R}) = \mathcal{N}\sum_{m}\left[\overline{\Gamma}^{\mu}(q)\right]^{-1}\overline{\Gamma}^{\mu}_{N,m}(q) \qquad \times$$

$$\langle m|\left(\frac{1}{\frac{-i\boldsymbol{\sigma}\cdot\boldsymbol{\nabla}}{E+\widehat{M}+\widehat{V}_s(\mathbf{R})-\widehat{V}_v(\mathbf{R})}}\right)e^{i\widehat{p}Z}\mathcal{P}\exp\left[\int_{-\infty}^{Z}dZ'\,\widehat{\Omega}(\mathbf{B},Z')\right]|N\rangle\chi_{-\check{\mathbf{s}}_R}, \tag{4.16}$$

where we have taken the momentum of the outgoing wavepacket to lie along the $\check{\mathbf{Z}}$ direction in Eq. (4.16) but not in the calculations. Again, $\mathcal{N} = \sqrt{(E+M_N)/(2M_N)}$. No sum over the index μ is implied in the above equation. Above, $\mathcal{P}$ is the path-ordering symbol. The effects of CT effects can be seen by comparing this expression with Eq. (3.13). We have projected the column vector $\boldsymbol{\Psi}$ on to the nucleon state to be detected, and could also project on to a nucleonic isobar to obtain the isobar production amplitude. The inelastic nucleon current operator, $\Gamma^{\mu}_{N,m}$, is defined in Eq. (4.3).

The expression for the CT wavefunction, shown in Eq. (4.16), is the central formal result of this paper. Note that we have changed the direction of the rest-frame spin projection, in accordance with Eq. (4.2).

1. Approximations: Vector OBO, LEE and EA

At this stage, we may proceed to make the expansions and approximations, as in Ref. [30], which allow a numerical evaluation of the CT wavefunctions, Eq. (4.16), the NCME, Eq. (4.15) and ultimately of the $(e, e'\vec{p})$ cross section. The definitions of these approximations are only slight generalizations of those in Ref. [30]. The "Order by Order" (OBO) scheme is defined by simply expanding the path-ordered exponential in Eq. (4.16) order by order in its Taylor series and evaluating the resulting matrix elements between the PLC and the nucleon. The Low-energy Expansion (LEE) scheme is defined by factoring out the expectation value of this operator $\widehat{\Omega}$ in the nucleon by letting $\widehat{\Omega}(\mathbf{R}) = \langle N|\widehat{\Omega}(\mathbf{R})|N\rangle + \Delta\widehat{\Omega}(\mathbf{R})$ and treating $\Delta\widehat{\Omega}$ as a perturbation. One must be a little careful, because of the presence of

the noncommuting Pauli matrices. We have also calculated the "Exponential Approxima-
tion" (EA) defined by exponentiating the first-order result of the OBO (this is equivalent
to neglecting the path ordering). This is similar to letting $1 - x \approx e^{-x}$. Our previous
experience leads us to believe that the EA and the LEE will be accurate at the low and
medium energies while the EA and the OBO should be reliable at the highest energies. This
is verified below.

V. MODEL EVALUATIONS AND APPLICATIONS

A. Wavepacket-Nucleon Interaction and Quark Space

To proceed further we need specific forms for $\widehat{f}$ and the states m. We choose the inter-
action to be

$$f(\widehat{b}^2) = \widehat{b}^2/b_H^2, \tag{5.1}$$

as in Eq. (4.5). Further, we choose the internal baryonic states to be described by a two-
dimensional transverse harmonic oscillator. For interactions of the form $f(\widehat{b}^2)$, the use
of three dimensional oscillators leads to the same results as those of the two-dimensional
case. We calculate transparencies for $b_H = 1\,fm$ and for two different values of the oscillator
spacing: $M_2^2 - M_N^2 = 1.19\,GeV^2$ and $M_2^2 - M_N^2 = 2.36\,GeV^2$. These simple choices reasonably
represent the present (lack of detailed) knowledge of $f(\hat{b}^2)$ and the baryon wavefunctions.
With the internal model space and interaction operator specified, we note the useful formula:

$$\langle 2m|\frac{\widehat{b}^2}{b_H^2}|2n\rangle = (2m + 1)\,\delta_{m,n} - m\,\delta_{m,n+1}$$
$$-(m + 1)\,\delta_{m+1,n}. \tag{5.2}$$

Before we describe our evaluations, it is necessary to show the parameters we use for
the strengths of the optical potentials. These are determined in Appendix A and displayed
in Table I. It is useful, when examining the table, to recall Eqs. (3.8) and (3.9). Also,
recall Eqs. (3.15), (3.16), (4.11) and (4.12) to see that at high energies the central potential
dominates and that, within the central potential, the vector potential is the important
quantity. Thus, we can immediately see that at high energies the optical potentials we
display in Table I are absorptive as the usual optical potentials.

The last column of Table I shows the potential strengths in nuclear matter in more conventional units, where we have taken $\rho_0 = 0.166\,fm^{-3}$. The optical potential strengths are energy dependent, but this energy dependence is unknown for higher energies where there is no data. Therefore, we have no way to really know what the strengths should be at higher energies. The strengths are totally determined by NN scattering data, but they are functions of more than just the invariant cross sections, see Appendix A. Thus, *we only consider our calculation to be reliable at energies where enough data exists to at least allow an approximate determination of the strengths.*

As described in Appendix A, the strengths displayed in Table I can be arranged to give the proton-nucleon total cross section and the ratio of the real to imaginary parts of the forward scattering amplitude, α_f. These numbers are summarized in Table II.

Defining some more notation helps us proceed. First, we introduce the shorthand notation $U^{(i,j)}$ such that

$$\langle 2m|\widehat{U}_c(R)|2j\rangle \equiv U_c^{(2m,2j)}(R) \tag{5.3}$$

$$\langle 2m|\widehat{U}_{so}(R)|2j\rangle \equiv U_{so}^{(2m,2j)}(R). \tag{5.4}$$

In the above equation, it is understood that $U_c^{(2j\pm2n,2j)}$ vanishes for $n \geq 3$ while $U_{so}^{(2j\pm2n,2j)} \equiv 0$ for $n \geq 2$.

More explicitly, we can evaluate the matrix elements just defined in terms of the scalar and vector optical potentials, using Eq. (5.2). Evaluation of the spin-orbit potentials require a little more discussion. In particular, the inverse operator appearing in Eq. (4.12) is problematical because $\left[\widehat{M}, \widehat{V}_{s(v)}\right] \neq 0$. However, neglecting the operators $\widehat{V}_s(\mathbf{R})$ and $\widehat{V}_v(\mathbf{R})$ in this inverse operator is of the same order of approximation as those already made in deriving the eikonal approximation so that it is safe to replace

$$\left[E + \widehat{M} + \widehat{V}_s(\mathbf{R}) - \widehat{V}_v(\mathbf{R})\right]^{-1} \approx \left[E + \widehat{M}\right]^{-1}, \tag{5.5}$$

also in Eq. (4.16) to be consistent. In that case, we can obtain explicit representations for the spin-orbit CT potentials. As an example,

$$U_{so}^{(0,0)}(R) = \frac{1}{R}\frac{\partial}{\partial R}\frac{V_v(R) - V_s(R)}{E + M_N}, \tag{5.6}$$

$$U_{so}^{(2,0)}(R) = -\frac{1}{R}\frac{\partial}{\partial R}\frac{V_v(R) - V_s(R)}{E + M_2}. \tag{5.7}$$

19

The first few central CT potentials have the explicit representations

$$U_c^{(0,0)}(R) = 2EV_v(R) + 2M_N V_s(R)$$

$$+2V_s^2(R) - 2V_v^2(R), \tag{5.8}$$

$$U_c^{(2,0)}(R) = (M_N - M_2 - 2E) V_v(R)$$

$$- (M_N + M_2) V_s(R) - 4V_s^2(R) + 4V_v^2(R), \tag{5.9}$$

$$U_c^{(4,0)}(R) = 2V_s^2(R) - 2V_v^2(R). \tag{5.10}$$

where we have only displayed the nonzero CT potentials which are connected to the ground state (nucleon). Since only the spin-orbit terms enter with the spin operator, it is convenient to define

$$U_{cso}^{(2m,2j)}(\mathbf{R}) = U_c^{(2m,2j)}(R) - ipZ\, U_{so}^{(2m,2j)}(R). \tag{5.11}$$

It is also useful to define, here, a commonly appearing combination of the above CT potentials:

$$\mathcal{U}_{c(so)}^{(2j)}(\mathbf{B}, Z, Z') = \sum_{m=0}^{\infty} U_{c(so)}^{(2m,2j)}(\mathbf{B}, Z)e^{i(p_{2m}-p)(Z-Z')}, \tag{5.12}$$

In performing the calculations, one also encounters terms like $\frac{p}{p_{2m}}$ and $\frac{E+M_N}{E+M_{2m}}$ which appear inside the summation sign above. In the spirit of the high-energy nature and approximations of this paper, in the calculations we assume all of these quantities to be equal. Thus, the expressions appearing in Eq. (5.6) and Eq. (5.7) are opposites in this approximation. The differences introduced by these approximations are smaller than the other uncertainties in the calculation.

B. Dirac Effects

We point out some interesting results obtained with this Dirac formalism. This is included in anticipation of the numerical results discussed below. The following effects are general features of a relativistic description of the wavepacket.

1) The presence of the commutator term in Eq. (4.11) causes a new non-Hermiticity in $\widehat{U}_c(R)$. Thus, care must be taken in order to obtain the correct sign of the commutator term.

Because of the quark operator structure present in $\widehat{U}_c$, and in $\widehat{U}_{so}$, it is a little bit tricky to switch between outgoing wave and incoming wave boundary conditions. In the DWBA, all we do is take the complex conjugate of the potentials. Here, that will not suffice. One must take the complex conjugate of the strengths, while leaving the CT part alone, except for making the change in this commutator term. Because this switch is complicated and relatively subtle, we only consider outgoing wave boundary conditions. We have checked, however, that both descriptions give the same result. Hereafter, this equality is to be understood and we drop the superscripts indicating the boundary condition.

2) The presence of the quadratic terms in the central potential causes an inequality between quantities $U_c^{(0)}(R)$, as defined in Eq. (4.11), and $U_c(R)$ as defined in Eq. (3.15). This effect is an artifact of the way we solve the Dirac eikonal formalism.

3) The commutator term in $\widehat{U}_c$ alters the approach to full transparency. This is seen in the following way. In the limit of zero size wavepacket, the inelastic and elastic form factors are equal. Then, we can neglect the subscripts on F_1, F_2 and Γ^μ. In that case, the initial PLC is described simply by $|PLC\rangle = \widehat{T}_H^\mu(q)|N\rangle = \Gamma^\mu(q) \sum_m |m\rangle$. Then,

$$\langle PLC|\widehat{U}_c(R)|N\rangle = \Gamma^\mu(q) \sum_m \langle m|\widehat{U}_c(R)|N\rangle, \tag{5.13}$$

$$= \Gamma^\mu(q)\Delta M \left(V_s(R) + V_v(R)\right), \tag{5.14}$$

where $\Delta M = M_N - M_2$. The reader is urged not to panic, however, despite the appearance that in the closure limit CT is not obtained. Upon looking at the definition of the CT potentials which actually enter, Eq. (4.13), we see that $\widehat{U}_c$ always enters with a factor of $\widehat{p}$ in the denominator. Thus, in the high-energy limit (closure limit) $\widehat{p} \approx p \to \infty$, the exponential factors do not matter, and the $\frac{1}{p}$ factor will suppress Eq. (5.14). This is not unlike the situation in Ref. [30]. In that case, the approach to transparency was described as $1 - e^{i(p_2-p)\Delta} \sim (p_2 - p)\Delta$ for large energies. Since $\widehat{p} \approx p + (M_N^2 - \widehat{M}^2)/(2p)$, we see that $p_2 - p \sim (M_N + M_2)(M_N - M_2)/p$. So, we see that CT is still obtained at very high energies, only its approach is affected. Furthermore, the terms which are left over, in the CT limit, are of the same order as terms like p/p_{2j} which we have neglected already.

4) New color transparency derivative (CTD) effects enter. To illustrate this effect, consider the one-dimensional functions

$$F(Z) = \int_{-\infty}^{Z} dZ' \, f(Z'), \tag{5.15}$$

$$F_{CT}(Z) = \int_{-\infty}^{Z} dZ' \, f(Z') \left[1 - e^{i(p_2 - p)(Z - Z')}\right]. \tag{5.16}$$

If the energy in this fictitious problem is low enough so that the momentum p_2 is below threshhold and thus purely imaginary, then it is true that

$$F_{CT}(Z) \overset{E \to M^+}{\Rightarrow} F(Z), \tag{5.17}$$

assuming that $Z - Z'$ is "large enough" to kill the exponential. Now, if we take the derivative with respect to Z we see that

$$F'(Z) = f(Z), \tag{5.18}$$

$$F'_{CT}(Z) = 0, \tag{5.19}$$

in the low-energy regime where the exponential will be damped because we are below threshhold. So, we are faced with the very interesting example of two functions which approach each other as $E \to M^+$ but whose derivatives do not. These CTD effects are relevant for the Dirac formalism used here because of the derivative $(\boldsymbol{\sigma} \cdot \boldsymbol{\nabla})$ which appears in the lower component of the Dirac wavefunctions. This effect is small

5) The Dirac strengths have a significant real part. The reader may be confused by the difference between our approach and the usual procedure of using the optical theorem to relate the strength of the optical potential to the cross section. (There the real part of the scattering amplitude causes negligible effects.) Here we convert the usual scattering amplitudes into their invariant Dirac form to extract the strengths of the scalar and vector potentials. Even when the real part of the forward scattering amplitude is neglected, the real parts of the Dirac strengths do not vanish. To illustrate this effect, we define a quantity

$$\Omega_v(\mathbf{R}) = -i \int_{-\infty}^{Z} dZ' \left(F^0_{v,r} - i F^0_{v,i}\right) \rho_v(\mathbf{B}, Z')$$
$$\times \left[1 - e^{i(p_2 - p)(Z - Z')}\right] \tag{5.20}$$

as a typical term in the CT equations which will dominate at high energies. Let us further define the integrals above to be

$$C_R(\mathbf{B}, Z) = \int_{-\infty}^{Z} dZ' \rho_v(\mathbf{B}, Z')$$

$$\times \left[1 - \cos(p_2 - p)(Z - Z')\right], \tag{5.21}$$

$$S_R(\mathbf{B}, Z) = \int_{-\infty}^{Z} dZ' \rho_v(\mathbf{B}, Z') \sin(p_2 - p)(Z - Z'), \tag{5.22}$$

so that

$$\Omega_v(\mathbf{R}) = -F_{v,i}^0 C_R(\mathbf{R}) - F_{v,r}^0 S_R(\mathbf{R})$$

$$+iF_{v,i}^0 S_R(\mathbf{R}) - iF_{v,r}^0 C_R(\mathbf{R}). \tag{5.23}$$

Now, in the previous approach, it was as if $F_{v,r}^0$ were zero. In that case, since C_R is positive definite, $e^{|\Omega_v|^2}$ was less than unity. Because our strengths have a significant real part and because S_R is not positive definite, it is possible to obtain $e^{|\Omega_v|^2} > 1$. Therefore, transparencies greater than unity are not disallowed.

The precise size of this nuclear enhancement effect depends in detail upon the relative sizes and phases of C_R and S_R as well as the strengths of the optical potentials. Thus, we cannot predict for certain that the cross section ratios will exceed unity at presently feasible energies, although we believe, on the grounds of the above argument, that this must eventually happen.

C. Zero Size

We also assume that the hard interaction forms a PLC. Then,

$$\langle N|\widehat{T}_H^\mu(q) = \sum_m \Gamma_{N,m}^\mu(q)\langle m|, \tag{5.24}$$

$$= C^\mu(q)\langle \mathbf{b} = 0| \tag{5.25}$$

where $\Gamma_{N,m}^\mu(q)$ is defined in Eq. (4.4). Using the specified model, all of the form factors are equal and we can neglect the subscripts on F_1, F_2 and on Γ^μ ($\Gamma^\mu \equiv \Gamma_{N,N}^\mu$). Then, $(\Gamma^\mu)^{-1}\Gamma_{N,m}^\mu = 1$. Later on we shall return to the case where the inelastic form factors are not equal to the elastic ones. In particular, in this Dirac case, interesting effects arising from a possible different F_1 and F_2 dependence on the size of the wavepacket are possible.

It is simple to obtain explicit evaluations of Eq. (4.16) within the various approximation schemes we have described. The results are lengthy; the interested reader can find them

in Appendix B. With explicit expressions for the wavefunctions in hand, we use Eq. (4.15) to calculate the nuclear current matrix element, from which we can construct the nuclear tensor and all of the observables.

VI. DISCUSSION OF NUMERICAL RESULTS

We have displayed the nuclear current matrix element (NCME), in Eq. (4.15), as a three-dimensional integral, with another integral to be performed in the wavefunction itself, for each order in perturbation theory. In the basis where $d^3R = BdB\,dZ\,d\phi$, the ϕ integral can actually be done exactly and analytically [34], but the result is not useful. Therefore, we simply perform all of the necessary integrals numerically. We must include 50 integration points per integral, using Gaussian quadrature to get stable numerical results.

The displayed results use kinematics closely related to that of the proposed experiments [8,9]. We do not use precisely those kinematics because our optical potential strengths are only known at energies where previous free NN data has been taken. Predictions for the upcoming experiments can be readily obtained using simple interpolations. These kinematics are summarized in Table III. For all of our calculations, we take the angle $\beta = \pi/2$ and consider only in-plane scattering. The quantities E_i and θ_e denote the initial electron energy and the electron scattering angle, respectively.

1. Convergence of Exponential Approximation

From our previous experience in Ref. [30], we learned that the exponential approximation (EA) was a good approximation to the full multiple-scattering series. This was seen by examining the higher order terms in the various approximation schemes and showing that all of the schemes converged to the EA in the energy regime where they were expected to be valid. The interpretation of the success of the EA is that the neglect of the path ordering includes many more higher-order terms than one would naively expect. We do not expect this conclusion to change simply by changing over to a Dirac description. To be careful we check to see if this remains true.

We calculate the total cross section ratios for the various approximation schemes described above, *in the forward direction only* to cut down on the computational time required. This should be a sufficient test. In Figures 3 and 4 we display the second-order cross section calculations in the forward direction, for two values of the internal (quark) oscillator spacing. To avoid distraction by the energy dependence of the elementary proton-proton scattering amplitude, we fix the optical potential strengths at their $Q^2 = 5.96\,GeV^2$ values. Further, we have calculated these results at the values $Q^2 = 1, 2, 3, 4, 5, 6, 8, 10, 12, 14, 16, 20, 25$ and $30\,GeV^2$.

We see that the exponential approximation (EA) is a good approximation to the true answer. At low energies, the LEE_1 follows the EA from the lowest energies to $Q^2 \approx 7\,GeV^2$ for a light excited state mass and up to $Q^2 \approx 12\,GeV^2$ for a heavy mass. The second-order LEE_2 does even better than the LEE_1 at higher energies and approaches the EA. It is clear that if one were to keep including higher orders in the LEE expansion, we would improve the higher energy results. At lower energies, the LEE_2 does not really converge to the EA as well as LEE_1. While one could argue that the agreement between the EA and the LEE_1 is accidental, we do not take this view. We believe that at the lower energy end, the LEE_2 is actually less accurate than the LEE_1. This is because we set p/p_{2m} equal to unity in our CT potentials, which is accurate at high energies. In a first-order calculation, because of the presence of the quadratic terms, we have neglected terms like $(p/p_4 - 1)$. In the second-order calculation, we have ignored terms like $(p/p_8 - 1)$. This kind of effect should be especially sizable a low energies. In order to do this calculation more carefully, one should keep these "momentum fraction" terms. However, these terms are of the same order as terms which have been neglected in the eikonal approximation itself. Thus, to do a really careful job, one should also include the first non-eikonal correction to the scattering equations. We do not do this here. The only point about the LEE_2 we want to make is that at low energies it is approximately equal to the LEE_1 and the EA and at higher energies, it more closely approximates the EA than does the first-order calculation.

At the high-energy end, we see that the OBO_1 fails terribly, even for ^{12}C. Of course, we expect the OBO to be increasingly worse for heavier nuclei where the propagation lengths are longer. However, adding in the second-order contribution to the OBO we find very good

agreement for $Q^2 \geq 16\,(21)\,GeV^2$ between the OBO_2 and the EA, for light (heavy) excited state masses.

At low energies, we really believe the LEE (the LEE_1 in particular) and at high energies the OBO is defined to describe the correct physics. What the results in Figures 3 and 4 tell us is that the approximation schemes overlap so that we can have confidence that the EA is the correct answer from $Q^2 \approx 1$ to $7\,(12)\,GeV^2$ and from $Q^2 \geq 16\,(21)\,GeV^2$ for light (heavy) excited state masses. Although we have not calculated higher order terms we take the position, that with our previous experience in Ref. [30], we can believe that the EA is a good approximation to the full multiple-scattering series over the whole energy range.

2. Integrated Unpolarized Cross Sections

We next display results for the ratios of integrated unpolarized cross sections. That is, we calculate the total cross section, as in Eq. (2.19), and divide by the Born cross section, defined by using a Dirac plane wave for the outgoing proton wavefunction in Eq. (4.2). See Figures 5, 6 and 7.

The solid curves (circles) are the DWBA cross sections, normalized to the respective Born cross sections. The dotdashed curves (diamonds) denote the cross sections, including CT effects via the exponential approximation, for oscillator spacings of $\Delta M^2 = 1.19\,GeV^2$ ($M_2 = 1.44\,GeV$). The dashed curves show the cross section ratios, including CT effects via the exponential approximation, for an excited state mass of $M_2 = 1.80\,GeV$. See Table III for the electron kinematics.

There are several noteworthy features in the figures. The first is that the optical potential strengths, which are calculated from free nucleon-nucleon scattering data, naturally give a DWBA cross section ratio which is large at $Q^2 \approx 1\,GeV^2$ and decreases sharply with energy before reaching an asymptotic value. This can be understood by noting that the pp cross section is only $30\,mb$ at this energy. Thus, we have here an effect similar to the one of Frankfurt, Strikman, and Zhalov [62]. Recall, the NE-18 people took measurements at $Q^2 =1,3,5$ and $6.8\ GeV^2$. With an excited state mass parameter of $1.44\,GeV$ the cross section at $Q^2 \approx 3\,GeV^2$ is the same as at $Q^2 \approx 1GeV^2$, although at $Q^2 \approx 5$ and $7\,GeV^2$ the cross section rises rapidly with energy.

We want to stress, at this point, that the precise value of the oscillator parameter, which controls the value of the excited state masses in the CT models, is unknown except for the fact that is on the order of hadronic mass differences.

Therefore, by simply increasing the value of the first excited state mass, we can postpone the onset of transparency to higher energies, see the dashed curves. The suppression of the transparency for an excited state mass of $1.80 \, GeV^2$ may be too great to agree with the SLAC data at $Q^2 \approx 3 \, GeV^2$. Thus, it seems that an oscillator spacing such that $M_2 \approx 1.6 \, GeV$ would give a cross section ratio which would appear to be Q^2-independent if one only looked at $Q^2 = 1, 3, 5, 6.8 \, GeV^2$.

The SLAC data are taken at kinematics slightly different than what we use. However, for cross section ratios, the differences in the electron kinematics lead to essentially the same results.

That the SLAC experiment has seen CT is certainly possible, given the energy dependence of the elementary pp cross section and the optical potential strengths. However, before one can be absolutely sure, it is desirable to take more data points and see what happens at, say, $Q^2 \approx 2 \, GeV^2$. It would also be nice to increase Q^2 and really see a dramatic rise in the ratio σ/σ^B.

3. Integrated Longitudinal and Transverse Responses

It has long been known that the longitudinal response function is suppressed relative to the transverse response in the quasi-elastic region [63–68]. The theoretical interpretation of this quenching has been difficult and no consensus, beyond the failure of naive applications of traditional nuclear theory, has yet been achieved. In particular, it has been suggested that a modification of the properties of the nucleon in medium or the presence of non-nucleon degrees of freedom is responsible for this suppression. It has also been suggested that relativistic effects may play a role. Indeed, Do Dang and Van Gai [63] have shown that the presence of large scalar and vector potentials in the nucleus may be responsible for this effect. Since our calculation is based on such a scalar-vector phenomenology, it is legitimate to ask whether or not our calculation displays this quenching.

As the integrated cross sections only involve the integrated longitudinal and transverse

27

response functions, Eq. (2.19), it is useful to examine the ratio of

$$\frac{\mathcal{R}_L}{\mathcal{R}_T} = \frac{\int d\zeta \, \sin\zeta \, R_L(\zeta)}{\int d\zeta \, \sin\zeta \, R_T(\zeta)} \approx \frac{\int dq_\perp \, q_\perp \, R_L(q_\perp)}{\int dq_\perp \, q_\perp \, R_T(q_\perp)}, \tag{6.1}$$

where ζ is the angle between the virtual photon and the ejected proton and $q_\perp = |\mathbf{p} - \mathbf{q}| \approx |\mathbf{q}| \sin\zeta$. Since the response functions R_L and R_T go to zero rapidly for $q_\perp \geq 1.5 \, fm^{-1}$, we take the limits of integration in $q_\perp$ to run from zero to some number $q_\perp^{max} \approx 2 \, fm^{-1}$. The contribution to the angle integrated responses $\mathcal{R}_{L(T)}$ from $q_\perp$ greater than $2 \, fm^{-1}$ is negligible. Note that this integration is over angle and *not* over the energy transfer. Thus, our ratio $\mathcal{R}_L/\mathcal{R}_T$ has very little to do with the integral involved in the Coulomb sum rule.

If longitudinal quenching occurs, $\mathcal{R}_L/\mathcal{R}_T < 1$. The dependence of this ratio as a function of Q^2, for quasi-elastic kinematics, can be inferred from the concept of $y-$scaling [16,69–75]. In order to determine the Q^2 dependence, we define the new reduced response functions r_L and r_T as

$$\mathcal{R}_L(\mathbf{q}, q_0) = \frac{A}{|\mathbf{q}|} \overline{G}_E^2(Q^2) \left(\frac{|\mathbf{q}|^2}{Q^2} \right) r_L(\mathbf{q}, q_0), \tag{6.2}$$

$$\mathcal{R}_T(\mathbf{q}, q_0) = \frac{A}{|\mathbf{q}|} \overline{G}_M^2(Q^2) \left(\frac{Q^2}{2M_N^2} \right) r_T(\mathbf{q}, q_0), \tag{6.3}$$

where $\overline{G}_E$ and $\overline{G}_M$ are the electric and magnetic form factors of the nucleus, which are weighted sums of the electric and magnetic form factors of the constituent protons and neutrons. The statement of y-scaling is that at large enough momentum transfers, the reduced response functions r_L and r_T are functions only of the variable

$$y = -\frac{|\mathbf{q}|}{2} + \frac{M_N \, q_0}{|\mathbf{q}|} \sqrt{\left(\frac{|\mathbf{q}|^2}{Q^2} \right) \left(1 + \frac{Q^2}{4M_N^2} \right)}. \tag{6.4}$$

The quantity y is to be interpreted as the longitudinal (parallel to $\mathbf{q}$) component of the initial nucleon momentum (in Born approximation) when the transverse (to $\mathbf{q}$) component is zero. We note that many choices of the scaling variable exist. At the top of the quasi-elastic peak $(x = Q^2/(2M_N q^0) = 1)$, $y = 0$ for all values of Q^2. Thus, in this kinematical limit, which is precisely where we have calculated, the functions r_L and r_T are independent of Q^2 (when y-scaling is valid). In principle, $r_L(y)$ and $r_T(y)$ should be equal. Experiments have found that although r_L and r_T seem to functions of y only, they are not the same function [73].

Thus, simply from looking at the remaining Q^2 dependence in Eqs. (6.2) and (6.3), we see that

$$\frac{\mathcal{R}_L}{\mathcal{R}_T} \overset{Q^2 \to \infty}{\to} \text{constant}, \tag{6.5}$$

from above. This is indeed what we see in our calculation.

In Figures 8, 9 and 10 we display the ratio $\mathcal{R}_L/\mathcal{R}_T$ as a function of Q^2 for ^{12}C, ^{40}Ca and ^{208}Pb. As before the circles, joined by solid lines, show this ratio for the DWBA calculation. The dotdashed curves (diamonds) and dashed (boxes) curves show this ratio for the CT-included cases (via the EA) for the light mass ($M_2 = 1.44\,GeV$) and the heavy mass ($M_2 = 1.80\,GeV$) cases. We also display the result for the plane wave or Born case, which is shown in the figures as the fancy boxes joined by the dotted curves.

At higher energies the CT-included ratios are slightly more suppressed than the DWBA. But only slightly. Thus, even if a careful Rosenbluth-type separation could be performed, the differences in $\mathcal{R}_L/\mathcal{R}_T$ predicted by the Glauber and CT calculations are too small to experimentally differentiate between the two.

4. Gauge Invariance and Current Conservation

We have mentioned earlier that our calculation violates gauge invariance and current conservation (CC). One of the main causes is that, in our NCME, we treat the bound state and scattered state as derived from different Hamiltonia and thus are not members of the same complete set. This is a typical problem for distorted wave calculations of this type. (For the initial- and final-state wavefunctions to be derived from the same Hamiltonian is necessary but not sufficient to obtain gauge invariance.) Gauge invariance is often imposed artificially [33,76]. In our view this is not the best solution, since one must be very careful to not introduce unphysical terms into the calculation. It is true that for our calculation to make any sense at all, the current must be at least approximately conserved. This subsection examines the question of CC.

There are many ways that one can consider quantifying the amount of current conservation violation (CCV). The nuclear current has four complex components, so directly looking at $q_\mu \mathcal{J}^\mu$ seems tedious. Instead, we consider the relevant elements of the nuclear tensor,

$\overline{W}^{\mu\nu}$. We would like to investigate how the CCV's change as a function of Q^2. Since $\overline{W}^{\mu\nu}$ is a function of angle $(q_\perp)$, we define

$$\overline{\mathcal{W}}^{\mu\nu} \equiv \frac{2\pi}{|\mathbf{q}|^2} \int dq_\perp \, q_\perp \, \overline{W}^{\mu\nu}. \tag{6.6}$$

where the energy-integrated nuclear tensor $\overline{W}^{\mu\nu}$ is defined by Eq. (2.5). The quantity $q_\perp = |\mathbf{p} - \mathbf{q}| \approx |\mathbf{q}| \sin\zeta$, where ζ is the angle between the the virtual photon and the ejected proton. Choosing the $\check{\mathbf{Z}}$-direction to be defined in the direction of $\mathbf{q}$, gauge invariance requires

$$\Delta R_L \equiv \frac{q_0^2 \overline{\mathcal{W}}^{00} - q_3^2 \overline{\mathcal{W}}^{33}}{q_0^2 \overline{\mathcal{W}}^{00} + q_3^2 \overline{\mathcal{W}}^{33}} \tag{6.7}$$

to be zero. We display results for ΔR_L as a function of Q^2 for our three canonical nuclei, ^{12}C, ^{40}Ca and ^{208}Pb, and for both internal oscillator spacings, $M_2 = 1.44\,GeV$ (light) and $M_2 = 1.80\,GeV$ (heavy).

We see, from looking at Figures 11, 12 and 13 that our calculation violates current conservation at the 10% level for the DWBA at the lowest energies but only at the 3-4% level for the CT cases. At higher energies, our calculation becomes more and more current conserving. Notice that the current is mostly conserved for the plane wave cases, becoming less so for the heavier nuclei.

Of course, in nature, current is conserved exactly. However, we make the provocative statement that the improvement of current conservation in our calculation over the traditional Glauber treatment is more evidence that CT effects are necessary for an accurate theoretical treatment of $(e, e'p)$ reactions.

5. Differential Cross Sections and Normal Polarizations

In this section, we display the results from our calculations for the differential cross sections (as a function of the transverse momentum) and of the normal polarizations. These are the quantities which will be measured in the upcoming CEBAF experiment [8,9]. We note that these are the first predictions of these observables at these energies which include the effects of CT. It is important to recall that, in the CT limit, the normal polarization should vanish.

We only display here, for reasons of space and continuity, some representative results for ^{12}C nucleus. The results for the other energies which we calculate and for ^{40}Ca and ^{208}Pb are presented in Ref. [77]. Here, the quantity E_i is the initial energy of the incident electron. Different values of E_i affect only the kinematical weights used to construct the cross section and polarization; the nuclear response functions are independent of the electron kinematics.

Clearly visible, in Figures 14 and 15, in the shapes of the differential unpolarized cross sections is the shell structure of the nucleus. For instance, ^{12}C has 4 p-shell protons and only 2 s-shell ones. The wavefunctions for the s-shell nucleons peak at the origin, of course, while the p-shell ones have a node there. This is the reason why the cross section for ^{12}C has a maximum at about $q_\perp \approx 0.5\,fm^{-1}$. Similarly, the shell structure for ^{40}Ca and ^{208}Pb can be discerned from the figures in Ref. [77].

We predict that the energies proposed in the experiments are **not** high enough to see the normal polarization vanish. However, in ^{12}C there is a measurable suppression of the polarization for the CT-included case of light excited state mass $(M_2 = 1.44\,GeV)$. A detailed comparison with the results of the SLAC NE-18 measurement of cross section ratios is necessary to see if using the light excited state mass is still viable. Our preliminary results are that using such a low mass may not be inconsistent with the SLAC NE-18 data. In ^{40}Ca and ^{208}Pb, there is only a small suppression of the normal polarization even at $Q^2 = 20\,GeV^2$.

Thus, it seems that the normal polarization is a difficult quantity in which to observe CT effects. But a precise experiment could be successful.

Note that our formalism does indeed yield vanishing normal polarization at high energies. To see this we look at the observables at $Q^2 \approx 300\,GeV^2$, with optical potential strengths fixed at their $Q^2 = 5.96\,GeV^2$ values. At this extremely high energy, the EA wavefunction is essentially the same as the OBO_1 wavefunction and the normal polarization is seen to be essentially zero for ^{12}C over the range in $q_\perp$ we consider, although for ^{40}Ca and ^{208}Pb the polarization is still sizeable at the larger angles, even at this enormous energy.

In Figure 16 we show the predictions from the $DWBA$ and the Born approximation (BA). The Born cross section is larger in magnitude than the $DWBA$ while the polarization is identically zero for the BA. The dotdashed curve is the prediction from the exponential

approximation, as before. The dotted curve is the prediction for the LEE_1 and the dashed curve is for the OBO_1. In all the CT curves, we have used an excited state mass parameter of $M_2 = 1.44\,GeV$. Much of the differences between the figures for different electron kinematics is due to the huge difference in the Mott cross sections, see Table III. There is also a sizeable difference in V_T. However, it is important to note that all of the $Q^2 = 5.96\,GeV^2$ results lead to cross section ratios which are the same to better than 1%. Since absolute magnitudes of the cross sections are larger for the greater incident electron energies, due to the Mott cross section, these kinematics are preferred experimentally. It is also interesting to comment on the OBO_1 curve. We see that the OBO_1 is, already at $Q^2 = 5.96\,GeV^2$, predicting a suppression of the normal polarization. We know that the OBO_1 is definitely inaccurate at these low energies. However, the high-energy nature of the approximation manifests itself in giving small polarizations.

6. Differential Unpolarized and Normal Response Functions

In this section we display representative graphs of the separated response functions, see Figures 17 and 18. Using these response functions, the total differential cross sections and normal polarizations can be constructed by summing them together with appropriate kinematical weights, given by the V's.

Since these quantities are more difficult to extract than the total differential cross sections and polarization, and Saha [8,9] is not planning to do so, we only display a few representative figures. The reader who is interested in more results of this kind are referred to Ref. [77].

We see from looking at the response functions that nothing really special happens for the "unpolarized response functions". Response functions represent spin-dependent or spin-independent measurements. It is convenient to adopt the phrases "unpolarized response" and "polarized response" or "normal response" to indicate the spin-independent or spin-dependent (dependent on normal component) responses.

In lead, there is strong absorption and the effects of CT do not manifest themselves until very high energies, making the experimental verification of CT in lead unlikely if one looks only at unpolarized observables. However, in the normal responses, we see something quite different and quite interesting. In the transverse normal response, R_T^n, we see that for

both light and heavy excited state mass cases there is a huge enhancement in the region of $q_\perp \approx 0.4 - 1.5 \, fm^{-1}$. That is, a ratio of CT response to DWBA response ranges all the way from zero to infinity over this angular range.

We note that this CT effect in R_T^n is not of the asymptotic nature one normally thinks of as CT, lack of absorption, something going to zero, etc. However, if one takes the CT wavefunctions we have derived seriously, then the low energy spin observables are affected in this way. In this sense, this enhancement in R_T^n is a pre-asymptotic effect of CT. This effect is also present in ^{40}Ca and in ^{12}C but to a lesser, and still lesser, extent.

If detected, this enhancement in R_T^n would be an unambiguous signature of CT. We stress that this enhancement begins at momentum transfers as low as $Q^2 \approx 2 \, GeV^2$ (!) and continues to the highest energies. However, the separation of this response function from the total normal polarization may be difficult. The kinematical weights, at these energies and angles, are all approximately equal, see Table III, so that the transverse normal response only contributes about one part in twenty to the polarization. The predictions presented here indicate that attempting this separation may be worthwhile.

A. Other Applications

1. Finite Size Effects

In all of the above calculations we have assumed that the wavepacket formed in the initial hard collision was of exactly zero size. This is not realistic. We do expect, however, that the size of the wavepacket will decrease with increasing momentum transfer. It is interesting to take this non-zero size into account. This is done by first considering the form factors defined in Eqs. (4.3) and (4.4) to be the product of the usual form factors with the internal part factored out. Further, we assume that the Dirac and Pauli form factors have the same internal dependence. That is, we take

$$F_{1N,2m}(q^2) = F_1(q^2)\frac{f_{N,2m}(q^2)}{f_{N,N}(q^2)}, \tag{6.8}$$

$$F_{2N,2m}(q^2) = F_2(q^2)\frac{f_{N,2m}(q^2)}{f_{N,N}(q^2)}. \tag{6.9}$$

In the absence of a compelling reason, note that we choose the internal dependence for F_1 and F_2 to be the same. With this simplification, the internal form factors simply factor out and (no sum over μ)

$$[\Gamma^\mu(q)]^{-1} \, \Gamma^\mu_{N,2m}(q) = \frac{f_{N,2m}(q^2)}{f_{N,N}(q^2)}, \tag{6.10}$$

which is proportional to the unit matrix in Dirac space. Now, to first order in the interactions, we identify as the relevant quantities

$$\mathcal{U}^{(2j)f}_{cso(so)}(\mathbf{B}, Z, Z') = \sum_m \frac{f_{N,2m}(q^2)}{f_{N,N}(q^2)}$$
$$\times U^{(2m,2j)}_{cso(so)}(\mathbf{B}, Z) e^{i(p_{2m}-p)(Z-Z')}, \tag{6.11}$$

where it is understood that, to the present order, only $m = 0, 1, 2$ are nonzero. In order to obtain explicit expressions for the internal form factors, we need to further specify the internal part of the hard scattering operator. It is generally believed that the size of the wavepacket is inversely proportional to the momentum transfer of the virtual photon. Suppose a nucleon, comprised of three quarks absorbs a photon of three-momentum $\mathbf{q}$. Each quark, then, recieves approximately $|\mathbf{q}|/3$ of the photon's momentum. So, we use a form [78] for the internal part of the hard operator

$$\widehat{T}^\mu_H(q) = T^\mu_H(q) e^{-\widehat{b}|\mathbf{q}|/3}. \tag{6.12}$$

This form is suggested by caricatures of perturbative QCD calculations; see Eq. (1) of Ref. [24].

In that case, the internal form factors $f_{N,N}$, $f_{N,2}$ and $f_{N,4}$ are given by

$$f_{N,N}(x) = 1 - x\sqrt{\pi}e^{x^2} \, \mathrm{erfc}(x), \tag{6.13}$$

$$f_{N,2}(x) = -x^2 + \left(x^3 + \frac{1}{2}x\right)\sqrt{\pi}e^{x^2}\mathrm{erfc}(x), \tag{6.14}$$

$$f_{N,4}(x) = \frac{1}{2}x^4 + \frac{1}{4}x^2$$
$$+ \left(-\frac{1}{2}x^5 - \frac{1}{2}x^3 + \frac{1}{8}x\right)\sqrt{\pi}e^{x^2}\mathrm{erfc}(x), \tag{6.15}$$

where $x = x(q^2) = |\mathbf{q}|b_H/6$.

The results for non-zero initial wavepacket size are displayed in Figures 19 and 20. In Figure 5 we show the ratio of cross sections for ^{12}C as a function of Q^2. As before, the

34

solid line denotes the $DWBA$ (where finite size of wavepacket has no effect) and CT is included via the exponential approximation for both light ($M_2 = 1.44\,GeV$) and heavy ($M_2 = 1.80\,GeV$) excited state masses. We have also overlayed the zero size calculations for comparison. For both the light (diamonds, dotdashed) at heavy mass (boxes, dashes) cases, the curves including the finite size are slightly below the zero size cases. That the effect is small even for the case of the light excited state mass is an indication that assuming exactly zero size is not a bad approximation.

In Figure 20 we show the CT curves for the current conservation violation (CCV) quantity ΔR_L as a function of Q^2. We label the curves EA to indicate that the CT effects are calculated in the exponential approximation. The superscripts LT and HVY indicate the mass of the excited state, light (LT) or heavy (HVY). The subscripts FS stand for "finite size" and those curves have included these finite size effects in the manner described above. Thus, the dotdashed (dashed) curves should be compared with one another. Looking at Figure 20 we see that the effects of including finite size improve the situation as far as gauge invariance is concerned. Including the size of the initial wavepacket shows that the CT calculations are gauge invariant at the 2% level at low energies whereas the zero size calculations are current conserving at the 3% level, at low energies. However, the trend to make the calculation better obey the requirements of current conservation is encouraging. We can conclude that assuming the initial wavepacket to be of exactly zero size introduces only small errors and can therefore be considered a good approximation.

We do not display results for the finite-sized calculation of $\mathcal{R}_L/\mathcal{R}_T$ because there is no discernable difference in this quantity between the finite-sized curves and the zero-sized ones.

2. Fermi Motion

It has recently been argued [62,79–81] that the Fermi motion of the nucleons bound in the nucleus strongly enhances the effects of color transparency. Suppose, in the $(e, e'p)$ reaction, that the virtual photon three-momentum is labelled by $\mathbf{q}$ and the detected proton three-momentum is called $\mathbf{p}$. Suppose that we call $\mathbf{p} = \mathbf{q} + \mathbf{k}$. Sometimes $\mathbf{k}$ is called the "momentum of the struck nucleon". This is only true in Born approximation (the CT limit) because final-state interactions can influence the outgoing proton's longitudinal momentum.

In exactly quasi-elastic kinematics, the bound nucleon is treated as at rest and free and so $\mathbf{k} = 0$. Fermi motion allows (requires) $\mathbf{k} \neq 0$. In the above calculations, we have assumed that $\mathbf{k} = \mathbf{q}_\perp$ where $\mathbf{q}_\perp$ is very small in magnitude, $|\mathbf{p}| \approx |\mathbf{q}|$, and is purely transverse to $\mathbf{q}$. This assumption leads to the differential distributions in Section VI and in Ref. [77].

It has been shown [79–81] that the component of $\mathbf{k}$ which is parallel (or anti-parallel) to $\mathbf{q}$ has a huge numerical effect on the calculated transparencies. This section is devoted to an investigation of this effect in our models.

We let the component of $\mathbf{k}$ which is in the $\check{\mathbf{q}}$ direction to be called $k_\parallel$ Thus, $\mathbf{k} = k_\parallel \check{\mathbf{Z}} + \mathbf{q}_\perp$. When $\mathbf{q}_\perp = 0$ then $k_\parallel = y$, where y is the scaling variable introduced in Section VI 3. Non-zero values of $k_\parallel$ are especially important in (p, pp) reactions [62] because the experimental results of Refs. [3,4] are presented in terms of bins of $k_\parallel$. As noted earlier, a correct accounting of this effect, in the kinematics of the Brookhaven experiment, leads to a better understanding of the data [80].

We have calculated the cross sections and other observables for $Q^2 = 0.96$ and $20.86\, GeV^2$ for values of $k_\parallel = -150, -75, 0, 75$ and $150\, MeV$. In particular, we assume that $\mathbf{p} \cdot \check{\mathbf{Z}} = |\mathbf{q}| + k_\parallel$, where $\mathbf{q}$ is in the $Z-$direction. The results for the total cross section ratios, $\mathcal{R}_L / \mathcal{R}_T$, and the CCV measure ΔR_L are shown in Figure 21. In all of the figures we display four curves. The dotted curve is the Born approximation, the solid curve is the DWBA, and the dotdashed and the dashed lines are CT results for light and heavy excited state masses. In the plots for the cross section ratios, we display the ratios for the cross section at $k_\parallel$ divided by the Born cross section at that same value of $k_\parallel$, except for the Born curve, which is the cross section at $k_\parallel$ divided by the Born cross section at $k_\parallel = 0$. At low energies, the effect of finite $k_\parallel$ is pretty small on the cross section ratios, about 20%. At high energies, the effect is quite large for the CT cases, although still a small effect for the DWBA. However, nonzero values for $k_\parallel$ lead to a large reduction, over a factor of 2, in the Born cross section at low and high energies.

Another extremely interesting result from these calculations is shown in the measure of CCV. In particular, we see that as $k_\parallel$ moves away from zero, current conservation is violated more and more, reaching the 40% level for $|k_\parallel| = 150\, MeV$, at low energies. At higher energies, the situation improves so that the violations are at the 5% level. Clearly,

violations of 40% or more are intolerable and our calculation probably cannot be trusted there; we shall come back to this point later. Violations of 5% probably do not affect the physics too much. Thus, there is no problem in trusting our calculation at high energies or at small values of $k_\parallel$.

What is the cause of the big change in CCV, due to the non-zero $k_\parallel$? One can get a hint by looking at the nuclear current for scalar electrodynamics. In that case, the current can be written as

$$J^\mu \propto \int d^4p\, \phi_i(p)\, (p + p')^\mu\, \phi_f(p'), \tag{6.16}$$

where $\phi_i(p)$ is the momentum space bound state wavefunction and $\phi_f(p')$ is the scattered wavefunction. In the Born approximation where $\phi_f(p') = \delta^4(p' - p - q)$, the integral can be done simply. The initial nucleon momentum p can now be indentified with k, defined above. Then, the statement of current conservation is that

$$q_\mu J^\mu \propto k_\parallel |\mathbf{q}|, \tag{6.17}$$

should vanish. We have used that $k_\mu k^\mu \approx M_N^2$ and chosen $x = Q^2/(2M_N q^0) = 1$. Therefore, we see that for vanishing $k_\parallel$ the current should be exactly conserved. Including the spin degrees of freedom makes this no longer exactly true, but this explains why the Born approximation is the most current conserving of our models. This also explains why, as $k_\parallel$ gets bigger, the violations of current conservation also grow. For large Q^2, we find that $q_\mu J^\mu \propto Q^2 k_\parallel / M_N \left[1 + \mathcal{O}(M_N^2/Q2)\right]$, which explains why the calculations become more gauge invariant at larger energies. For non-zero $k_\parallel$ the above argument indicates that the current is not conserved. Why not? Obviously, something is missing in our calculation. The most important cause of CCV in our calculation is probably coming from the lack of orthogonality between the initial state and final-state wavefunctions. Indeed, we have left out effects in the initial state, such as particle-hole excitations as well as explicit isobar degrees of freedom which can alter the nucleon-nucleon force. Also, we have ignored the possibility that the nucleons are altered at all in the medium. Further, our assumption that the current operator is the free nucleon operator is probably not warranted; off-shell effects may be important. A more careful treatment of some of these effects could lead to improvements in the gauge

invariance of our models. The source of these CCV's are of much interest and deserve further study in the future.

<center>*3. Lower Components*</center>

We examine the effects of the lower components of our model wavefunctions here. We only present results for the light mass case and for the ^{12}C nucleus.

First, we artificially turn off the lower components in the scattered waves. The results for the integrated cross section ratios are shown in Figure 22. The solid and dotdashed curves are calculated using the the DWBA and EA wavefunctions with the lower components turned off, divided by the Born calculation also with no lower components. The dotted curve in Figure 22 is the ratio of the Born calculation with no lower components to the Born calculation with lower components. The figure shows a striking effect: the lower components are not significant in the predicted cross section ratios. These cross section ratios are seen to be a quantity which is very insensitive to the details of the wavefunctions. This is actually quite amazing since the Born calculation changes so much when the lower components are turned off.

However, we point out that these lower components are crucial to the approximate satisfaction of current conservation, see Figure 23. Further, turning off the lower components has a huge effect on the integrated ratio of longitudinal to transverse response, see Figure 24. Thus, we see that the suppression of the longitudinal response relative to the transverse response is really entirely located in the lower components. This is consistent with the notion, mentioned earlier, that this longitudinal quenching was due to relativistic effects. Naturally, since this ratio is quite different than previously, all of the other observables such as differential unpolarized cross sections, differential normal polarizations and differential response functions are also altered by a large amount.

We have also performed a calculation in which we take the ratio of lower to upper components in the scattered wave to be the same as for a free Dirac plane wave, $\frac{\sigma \cdot \mathbf{p}}{E+M}$. This replacement has essentially no effect on any of the observables at the energies we consider. Only the ΔR_L is altered noticeably, with the DWBA violating the current conservation a little more ($\sim 5 - 10\%$) without lower components than with them and the EA conserving

<center>38</center>

the current a little bit more. These results show that the CT derivative effects, described in Section V B, are not numerically significant and practically all of the physics is independent of these CTD's in the lower components. Since the differences are small we do not display any numerical results for this calculation.

We also investigate turning off the lower components in the bound state wavefunction. This change introduces only very small corrections to the observables and has only a small ($<$ 5%) effect on the level of current conservation violations; the changes in the other observables are not important. This is consistent with our expectation; the QHD bound state lower components contribute only $2 - 3\%$ to the total probability. That is, $\int dr |F|^2 / \int dr |G|^2 \approx 0.02 - 0.03$. We do not display any numerical results for this calculation, either.

We conclude that the lower components are essential to our description of the ejectile wavefunction. Without these inherently relativistic components we would lose approximate current conservation and the experimentally observed quenching of the longitudinal response, although the integrated cross section ratios remain unchanged. However, examination of the details shows that the dominant effect in the lower components of the wavefunctions is the $\sigma \cdot \mathbf{p}$ term and that the complicated terms which appear in the explicit evaluations of the wavefunctions are unimportant.

We have also explored the effects of changing our bound state wavefunction. Instead of using the QHD wavefunction of Horowitz and Serot [38], we use harmonic oscillator wavefunctions. Using these bound state wavefunctions leads to only very small changes in the cross section ratios and in the violations of current conservation. However, the differential cross sections are slightly different than those presented in Section VI 5. This is because the $p-$wave wavefunction has a smaller $\langle R^2 \rangle$ (higher momentum components) than the corresponding QHD wavefunction. As a result, the differential cross section calculated from this oscillator wavefunction peaks at a larger value of $q_\perp$ and has smaller contribution at low $q_\perp$. The contribution to the differential cross section from the $s-$wave fall faster than the increasing contribution from the $p-$wave, so that the bump that we saw in the QHD case disappears.

It is possible to fix the $\langle R^2 \rangle$ for the harmonic oscillator wavefunctions to agree with that predicted by the QHD model. Doing this improves the agreement between the $p-$waves but

at the expense of the agreement between the $s-$waves. Thus, the differential cross sections seem to be sensitive to the precise form of the bound state wavefunctions.

However, the main conclusion of this work on polarization, that the normal polarization is not hugely suppressed at present energies, remains unchanged when harmonic oscillator bound states are used.

VII. SUMMARY AND CONCLUSIONS

The effects of color transparency (CT) in quasi-elastic $(e, e'p)$ reactions at large momentum transfers are explored here. We have focused on the $(e, e'p)$ reaction since lepton scattering is simpler than hadronic scattering. Of course, CT effects should also be present in other reactions such as (p, pp), $(\pi, \pi p)$, etc. The methods presented in this paper can be applied to these reactions.

In this paper we include the effects of proton and photon spin. Thus, we call this work "Vector CT", reflecting the vector nature of the photon. So far no published work has included the effects of spin in calculations of CT. The main motivation for undertaking this calculation is the proposal by Saha and collaborators [8,9] who plan to measure the normal component of the proton polarization in $(e, e'\vec{p})$ experiments. This polarization is an interesting quantity because it vanishes in the absence of final-state interactions. Further, the photon really is a vector particle and its spin should play some role in the scattering. Dirac phenomenology is used to construct the DWBA. The internal operators and states are then embedded in to this formalism. We obtain detailed expressions for the CT wavefunction in terms of these internal operators.

In order to calculate the CT effects, it is necessary in this approach to choose an explicit form for the wavepacket-nucleon interaction. Although this interaction is not precisely known, some general properties are generally agreed upon. We choose a simple representative form for this interaction which is consistent with the known constraints.

Further, it is also necessary to assume a model for the internal space on which the CT operators act. For simplicity, we choose the baryon spectrum to be represented by a two-dimensional transverse harmonic oscillator. With this choice comes a single free parameter, the oscillator spacing, which determines the masses of the nucleon resonances. This spacing

is characterized by the mass of the first even parity excited state, which we label by M_{N^*}. In this paper, we have chosen the values $M_{N^*} = 1.44\,GeV$ and $M_{N^*} = 1.80\,GeV$ for the numerical results we display. Increasing this mass postpones the onset of CT to higher energies.

We evaluate the formal distorted wavefunction by making various approximations to sum up different parts of the multiple-scattering series. In each energy regime we define an unperturbed piece of the path-ordered exponential, which we can solve exactly, and a perturbed piece, which we treat systematically in perturbation theory. We have developed high-energy and low-energy approximations. However, the different approximation schemes overlap so that we are confident that we can accurately approximate the exact distorted wavefunction at all energies (above 1 GeV). In particular, we find that simply ignoring the path ordering symbol in the wavefunction serves as a good approximation of the full distorted wavefunction for all energies.

Although we use over-simplified models for the wavepacket-nucleon interaction and the internal baryon space, the methods of calculation presented in this paper are more general and can be used with more realistic interactions and models.

We calculate ratio of cross sections for ^{12}C, ^{40}Ca and ^{208}Pb as a function of Q^2. In contrast to earlier calculations which assume a constant value of $40\,mb$ for the elementary proton-proton cross section, we take the cross section and other optical potential strengths directly from data. Thus, we confirm the assertion of Frankfurt, Strikman and Zhalov, that energy dependence in σ/σ^B is expected. This is because the pp cross section, in the energies of the experiment varies in such a way that the Glauber treatment decreases the transparency ratio. Therefore, since the preliminary results of the experiment, so far, see a small variation in the ratio as a function of Q^2, there may be some transparency effects to compensate. We conclude that the excited state mass which is consistent with the preliminary data is about $M_{N^*} \approx 1.6\,GeV$ or more.

A typical problem with calculations of this sort is the lack of current conservation. We show that the violations of gauge invariance are at the 10% level for the DWBA and only at the 4% level for the CT wavefunctions at low energies but are all at the $1 - 2\%$ level at the highest energies, $Q^2 \approx 20\,GeV^2$. Inclusion of CT effects is therefore desirable, even

at low energies, because it improves the situation from the DWBA with respect to current conservation and gauge invariance.

Because of the extra spin degrees of freedom, there are many many other quantities which we calculate. We display results for the ratio of integrated longitudinal to transverse response as well as for differential cross sections and normal polarizations. The differential cross sections do display a noticeable, and detectable, increase at large momentum transfers. This is just the data which is summarized in the integrated cross section ratios described above. In the normal polarizations, we see that the deviations from the usual Glauber treatment do not seem to be significant or measurable at any energy. Although $Q^2 \approx 20\,GeV^2$ we see, in ^{12}C a moderate decrease of the polarization for the light mass CT case but not for the heavy case. We conclude that the energies at which the normal polarization should completely vanish are, unfortunately, quite high. Frankfurt, Strikman and Zhalov have obtained a similar result (private communication).

We have also calculated the individual separated response functions, eight in all for in-plane scattering, which require many measurements at many angles in order to accurately extract from the cross sections and polarizations. We notice, in some of the response functions, that some pre-asymptotic behavior of the CT wavefunctions are manifest are possible detectable. This is an effect which increases in heavy nuclei like ^{208}Pb. In particular, if it is possible to separate out from the normal polarization the responses R_L^n, R_T^n, R_{TT}^n and R_{LT}^n, then it should be possible to see in R_T^n a *huge* enhancement over the Glauber result at $|\mathbf{q}_\perp| \approx 0.5 - 1\,fm^{-1}$ for $Q^2 \geq 2\,GeV^2$!. This extraction may be difficult because, although the kinematical weights are all approximately equal, R_T^n contributes only about one part in ten at most to the total polarization.

Further, we have also investigated the effects of non-zero wavepacket size and of Fermi motion. Including the non-zero size of the initial wavepacket produces only small changes so its neglect is a very good approximation. This is because of effects of wave packet expansion. Very small sized wave packets expand quickly into small sized wave packets. However, a slight improvement in the current conservation is obtained by including the non-zero size. The Fermi motion, on the other hand, can have a big effect on the cross section ratios if the "initial nucleon momentum" is along the direction of $\mathbf{q}$. However, for values of $k_\parallel \gtrsim 150$

MeV/c, which is this component, the violations of current conservation become severe at low energies and our calculation cannot be trusted there. At high energies, the calculation becomes more gauge invariant and we see an interesting effect for non-zero $k_\parallel$. This effect is especially important for the (p, pp) reaction where the data is displayed in bins of $k_\parallel$ [80].

Lastly, we have also investigated the effects of the lower components on cross section ratios, current conservation, polarization, etc. The complicated nature of the DWBA and CT lower components are not significant and taking the ratio of lower to upper components for these distorted waves to be the same as for plane waves introduces no discernable results (CTD effects are unimportant). The bound state lower components are similarly seen to be unimportant in the prediction of most of the observables. Finally, we have investigated the effects of using harmonic oscillator bound states instead of the ones given by QHD. The cross section ratios are essentially the same as for the QHD bound states, while the differential cross sections, polarizations and response functions all differ somewhat from those using QHD bound states.

In conclusion, we can make the following short comments. The recent SLAC data [7] imposes constraints on the allowable models shown in this paper. Despite the lack of significant Q^2 variation in the data it is possible, because of the energy dependence of the elementary pp observables, that the data actually may be an example of the manifestation of CT. A measurement of the normal polarization in $(e, e'\vec{p})$ reactions does not seem to be a good way to see CT effects at moderate Q^2. However, a measurement of the normal transverse response in a heavy nucleus such as ^{208}Pb does seem to afford the opportunity to see CT, unambiguously, at quite low momentum transfers.

ACKNOWLEDGMENTS

REFERENCES

*   Present Address: Department of Physics, University of Pennsylvania, Philadelphia, PA 19104.

[1] A. H. Mueller, *Proceedings of Seventeenth Rencontre de Moriond*, Moriond, 1982, ed. J. Tran Thanh Van (Editions Frontieres, Gif-sur-Yvette, France, 1982) p13.

[2] S. J. Brodsky in *Proceedings of the Thirteenth Int'l Symposium on Multiparticle Dynamics*, ed. W. Kittel, W. Metzger and A. Stergiou (World Scientific, Singapore 1982,) p963.

[3] A. S. Carroll et. al. *Phys. Rev. Lett.* **61**, 1698, (1988).

[4] S. Heppelmann, p. 199 in *Nuclear physics on the Light Cone*, ed. by M. B. Johnson and L. S. Kisslinger, (World Scientific, Singapore, 1989).

[5] A. S. Carroll *et al.*, BNL expt. 850.

[6] SLAC Expt. NE-18, R. Milner and R. McKeown, spokesmen.

[7] R. McKeown, spokesman, NE-18 collaboration, at the 1992 Meeting of the Division of Nuclear Physics of the American Physical Society in Santa Fe, NM, October, 1992.

[8] A. Saha et. al., *Study of Nuclear Medium Effects by Recoil Polarization up to High Momentum Transfers*, CEBAF proposal PR91-006. Proposed and approved.

[9] A. Saha et. al., proposed experiment for the European Electron Accelerator Facility, *Study of Nuclear Medium Effects and the Onset of Color Transparency in Nuclei in the Q^2 range of 6 to 16 GeV^2*. A. Saha, private communication.

[10] K. S. Egiyan, L. L. Frankfurt, W. R. Greenberg, G. A. Miller, M. M. Sargsyan and M. I. Strikman, *Searching for Color Coherent Effects via Double Scattering Events*, CEBAF proposal PR93-002, 1993.

[11] F. E. Low, *Phys. Rev.* **D12**, 163 (1975).

[12] S. Nussinov, *Phys. Rev. Lett.* **34**, 1286 (1975).

[13] J. Gunion and D. Soper, *Phys. Rev.* **D15**, 2617 (1977).

[14] B. Povh and J. Hufner, *Phys. Rev. Lett.* **58**, (1987) 1612.

[15] G. Bertsch, S. J. Brodsky, A. S. Goldhaber and J. F. Gunion, *Phys. Rev. Lett.* **47**, 297 (1981).

[16] L. Frankfurt and M. Strikman, *Phys. Rep.* **160**, 235 (1988).

[17] B. Z. Kopeliovich, *Sov. J. Part. Nucl. Sci.* **21**, 117 (1990).

[18] L. Frankfurt and M. Strikman, *Progress in Particle and Nuclear Physics*, **27**, 135 (1991).

[19] L. Frankfurt, G. A. Miller and M. Strikman, *Comm. Nuc. Part. Phys.* **21**, 1 (1992)

[20] H-n Li and G. Sterman, *Nucl. Phys.* **B381**, 129 (1992).

[21] L. Frankfurt, G. A. Miller, and M. Strikman, Nucl. Phys. **A555**, 752 (1993).

[22] G. R. Farrar, H. Liu, L. L. Frankfurt and M. I. Strikman, Phys. Rev. Lett. **61**, 686 (1988).

[23] B. K. Jennings and G. A. Miller, *Phys. Lett.* **B236**, 209 (1990).

[24] B. K. Jennings and G. A. Miller, *Phys. Rev.* **D44**, 692 (1991).

[25] G. A. Miller and B. K. Jennings p. 25 in *Perspectives in Nuclear Physics at Intermediate Energies* Ed. S. Boffi, C. Ciofi degli Atti, M. Giannini, (World Scientific, Singapore, 1992).

[26] G. A. Miller, in *Nucleon resonances and Nucleon Structure*, G. A. Miller, editor. (World Scientific, Singapore, 1992), p. 209.

[27] B. Z. Kopeliovich and B G. Zakharov, Phys. Lett. **B264**, 434 (1991).

[28] B. Z. Kopeliovich and B G. Zakharov, Phys. Rev. **D44**, 3466 (1991)

[29] M. Zhalov, private communication to A. Saha and M. Strikman.

[30] W. R. Greenberg and G. A. Miller, *Phys. Rev.* **D47**, 1865 (1993).

[31] A. Picklesimer and J. W. Van Orden, *Phys. Rev.* **C35**, 266 (1987).

[32] J. D. Bjorken and S. D. Drell, *Relativistic Quantum Mechanics* (McGraw-Hill, New York, 1964).

[33] A. Picklesimer and J. W. Van Orden, *Phys. Rev.* **C40**, 290 (1989).

[34] A. Allder, Ph.D. thesis, Caltech, 1992.

[35] A. Picklesimer, J. W. Van Orden and S. J. Wallace, *Phys. Rev.* **C32**, 1312 (1985).

[36] L. S. Celenza and C. M. Shakin, *Relativistic Nuclear Physics*, (World Scientific, Singapore, 1986).

[37] B. D. Serot and J. D. Walecka, *Adv. Nucl. Phys.* **16**, 327 (1986).

[38] C. J. Horowitz and B. D. Serot, *Nucl. Phys.* **A368**, 503 (1981).

[39] C. J. Horowitz, private communication.

[40] C. Itzykson and J. Zuber, *Quantum Field Theory* (McGraw-Hill, New York, 1980).

[41] L. G. Arnold, B. C. Clark, R. L. Mercer and P. Schwandt, *Phys. Rev.* **C23**, 1949 (1981).

[42] E. Rost, J. R. Shepard and D. Murdock, *Phys. Rev. Lett.* **49**, 448 (1982)

[43] R. D. Amado, J. Piekarewicz, D. A. Sparrow and J. A. McNeil, *Phys. Rev.* **C28**, 1663 (1983).

[44] J. Piekarewicz, R. D. Amado, D. A. Sparrow and J. A. McNeil, *Phys. Rev.* **C28**, 2392 (1983).

[45] J. Piekarewicz, *Phys. Rev.* **C32**, 1693 (1985).

[46] F. Cannata, J. P. Dedonder and J. R. Gillespie, *Nucl. Phys.* **A467**, 636 (1987).

[47] J. R. Shepard, J. A. McNeil and S. J. Wallace, *Phys. Rev. Lett.* **50**, 1443 (1983).

[48] J. A. McNeil, L. Ray and S. J. Wallace, *Phys. Rev.* **C27**, 2123 (1983).

[49] J. A. McNeil, J. R. Shepard and S. J. Wallace, *Phys. Rev. Lett.* **50**, 1439 (1983).

[50] S. J. Wallace, *Adv. Nuc. Phys.* **12**, 135 (1981).

[51] S. J. Wallace, *Comm. Nucl. Part. Phys.* **13**, 27 (1984).

[52] S. J. Wallace, in *Relativistic Dynamics and Quark- Nuclear Physics*, edited by M. Johnson and A. Picklesimer, p. 418, (J. Wiley & Sons, New York, 1986).

[53] S. J. Wallace *Ann. Rev. Nucl. Part. Sci.* **37**, 267 (1987).

[54] S. J. Wallace, private communication.

[55] N. Hoshizaki and T. Kadota, *Prog. Theor. Phys.* **42**, 815 (1969).

[56] N. Hoshizaki and T. Kadota, *Prog. Theor. Phys.* **57**, 335 (1977).

[57] N. Hoshizaki, *Prog. Theor. Phys.* **57**, 1099 (1977).

[58] N. Hoshizaki, *Prog. Theor. Phys.* **60**, 1796 (1978).

[59] Y. Higuchi and N. Hoshizaki, *Prog. Theor. Phys.* **62**, 849 (1979).

[60] M. Matsuda, H. Suemitsu, W. Watari and M. Yonezawa, *Prog. Theor. Phys.* **66**, 1102 (1981).

[61] M. Matsuda, H. Suemitsu, M. Yonezawa, *Phys. Rev.* **D33**, 2563 (1986).

[62] L. Frankfurt, M. Strikman and M. Zhalov, P.S.U. preprint "Pitfalls in Looking for Color Transparency at the Intermediate Energies," 1993.

[63] G. Do Dang and N. Van Giai, *Phys. Rev.* **C30**, 731 (1984).

[64] Z. E. Meziani, et. al., *Phys. Rev. Lett.* **52**, 2130 (1984).

[65] Z. E. Meziani, *Nucl. Phys.* **A446**, 113c (1985).

[66] H. Kurasawa and T. Suzuki, *Nucl. Phys.* **A445**, 685 (1985).

[67] B. Frois and C. Papanicolas, *Ann. Rev. Nucl. Part. Sci.* **37**, 133, (1987).

[68] C. J. Horowitz, *Phys. Lett.* **B208**, 8, (1988).

[69] G. B. West, *Phys. Rep.* **18**, 263, (1975).

[70] G. B. West, in *Electron and Pion Interactions with Nuclei at Intermediate Energies*,

edited by W. Bertozzi, S. Costa and C. Schaerf, p. 417, (Harwood Academic Publishers, New York, 1980).

[71] C. Ciofi degli Atti, *Il Nuovo Cimento* **76A**, 330, (1983).

[72] R. Lourie, in *Relativistic Dynamics and Quark- Nuclear Physics*, edited by M. Johnson and A. Pickleseimer, p. 482, (J. Wiley & Sons, New York, 1986).

[73] J. M. Finn, R. W. Lourie and B. H. Cottman, *Phys. Rev.* **C29**, 2230 (1984).

[74] D. B. Day, J. S. McCarthy, T. W. Donnelly and I. Sick, *Ann. Rev. Nucl. Part. Sci.* **40**, 357 (1990).

[75] I. Sick, *Comm. Nucl. Part. Phys.* **18**, 109 (1988).

[76] T. de Forest, *Nucl. Phys.* **A392**, 232 (1982).

[77] W. R. Greenberg, Ph.D. thesis, University of Washington, 1993.

[78] B. K. Jennings, private communication.

[79] B. K. Jennings and B. Z. Kopeliovich, "Color Transparency and Fermi Motion", TRI-UMF preprint, 1992, Phys. Rev. Letters.

[80] B. K. Jennings and G. A. Miller, "Natural Color Transparency in High Energy (p,pp) Reactions", submitted to *Phys. Lett.* **B**.

[81] A. Bianconi, S. Boffi and D. E. Kharzeev, "Colour Transparency in Hadronic Basis", University of Pavia preprint, 1993.

[82] M. L. Goldberger, M. T. Grisaru, S. W. MacDowell and D. Y. Wong, *Phys. Rev.* **120**, 2250 (1960).

[83] W. Grein and P. Kroll, *Nucl. Phys.* **B137**, 173 (1978).

[84] J. Bystricky, F. Lehar and P. Winternitz, *J. Physique* **39**,1 (1978).

[85] J. Bystricky, C. Lechanoine-Leluc and F. Lehar, *J. Physique* **48**, 199 (1987).

[86] C. D. Lac, et. al., *J. Phys. France* **51**, 2689 (1990).

[87] D. R. Rust, et. al., *Phys. Lett.* **B58**, 114 (1975).

[88] R. D. Klem, et. al., *Phys. Rev.* **D15**, 602 (1977).

[89] S. L. Kramer, et. al., *Phys. Rev.* **D17**, 1709 (1978).

APPENDIX A: EXTRACTION OF OPTICAL POTENTIAL STRENGTHS

We describe how we obtain the strengths of the scalar and vector optical potentials, first shown in Eq. (3.9), and summarized numerically in Table I. In particular, we extract these strengths from proton-proton elastic scattering data. In order to show exactly what we have done, it is useful to recall some aspects of nucleon-nucleon scattering.

1. Nucleon-Nucleon Scattering

We use the parameterization of the nucleon-nucleon scattering amplitude of [47–53],

$$\frac{f_c}{2ik} = A + B\boldsymbol{\sigma}_1 \cdot \boldsymbol{\sigma}_2 + iqC\left(\sigma_{1n} + \sigma_{2n}\right)$$
$$+ D\boldsymbol{\sigma}_1 \cdot \mathbf{q}\,\boldsymbol{\sigma}_2 \cdot \mathbf{q} + E\sigma_{1Z}\sigma_{2Z}. \tag{A1}$$

The amplitudes A, B, C, D, E can be easily related to the s-channel helicity amplitudes [82].

One can also parameterize the NN scattering amplitude in a Lorentz invariant form [47–53], by describing the spin dependence in terms of Dirac matrices,

$$F = F_s + F_v\gamma_1^\mu\gamma_{2\mu} + F_t\sigma_1^{\mu\nu}\sigma_{2\mu\nu} + F_p\gamma_1^5\gamma_2^5$$
$$+ F_a\gamma_1^5\gamma_2^5\gamma_1^\mu\gamma_{2\mu}. \tag{A2}$$

Naturally, the quantities F_s, F_v, etc. are functions of the momentum transfer, $\mathbf{q}$. By taking the matrix element of this operator and doing the Dirac algebra, leaving F to be an operator in the Pauli spin space, we can equate the two descriptions, modulo some kinematical factors. These factors are known and are derivable from the relativistic impulse approximation [47–53]. In fact, the relationship is, in the center-of-mass frame,

$$\chi_{\lambda_1'}^\dagger \chi_{\lambda_2'}^\dagger \frac{f_c}{2ik} \chi_{\lambda_1} \chi_{\lambda_2}, =$$
$$\overline{u}(\mathbf{k}', \lambda_1')\overline{u}(-\mathbf{k}', \lambda_2') \, F \, u(\mathbf{k}, \lambda_1)u(-\mathbf{k}, \lambda_2) \tag{A3}$$

49

where χ_λ are Pauli spinors for helicity λ and $u(\mathbf{k}, \lambda)$ are free Dirac spinors corresponding to momentum $\mathbf{k}$ and helicity λ; k is the center-of-mass momentum.

2. The Lorentz Invariant Forward Amplitudes

We are concerned with the case of elastic scattering of protons from nuclei. It is in this case that we can extract the optical potential strengths. Within the context of the relativistic impulse approximation, the T-matrix for nucleon-nucleus scattering is simply a sum of the t-matrices of the elementary nucleon-nucleon scattering. If we neglect nuclear-medium modification to the bound nucleons, off-shell effects, and $1/A$ corrections, the optical potential is approximately equal to the impulse approximation T-matrix [49]. In a spin saturated nucleus, the matrix element of this Dirac operator involves a trace over struck nucleon spins which eliminates all terms except the tensor, scalar and the time component of the vector terms. Thus, in this relativistic impulse approximation, the optical potential is of the form,

$$U_{opt}(\mathbf{q}) = -\frac{4\pi i p_{lab}}{M_N} \Big[F_s(q)\rho_s(q) + \gamma_1^0 F_v(q)\rho_v(q)$$
$$-\frac{\boldsymbol{\alpha} \cdot \mathbf{q}}{M_N} F_t(q)\rho_t(q) \Big], \tag{A4}$$

where ρ_s, ρ_v and ρ_t are scalar, vector and tensor nuclear densities and p_{lab} is the lab frame momentum. The kinematical factors on the right hand side of the above equation, $r \equiv -4\pi i p_{lab}/M_N$, come from the relationship between the Lorentz invariant Feynman amplitude and the usual description of the optical potential in the impulse approximation.

The coordinate space optical potential is obtained by Fourier transforming the momentum space potential. In the limit of very high energies, the scattering is predominantly in the forward direction. Thus, we can approximate $F_s(q)$ and $F_v(q)$ by their forward direction values F_s^0 and F_v^0, and neglect the tensor term since q is small. Thus, we arrive at [47,49]

$$U_{opt}(\mathbf{R}) = r \left[F_s^0 \rho_s(R) + \gamma_1^0 F_v^0 \rho_v(R) \right]. \tag{A5}$$

In the forward scattering approximation, the relationship between the Pauli and Dirac amplitudes can be written as a matrix equation [48]. Since A, B, C, D, E are to be taken

directly from data, we can simply invert this matrix to obtain the scalar and vector density strengths from the Pauli amplitudes. In particular, we find

$$F_s^0 = \frac{1}{2\xi^2(1+\xi)}\Big[\xi(2\xi+1)A^0 + (2\xi^2-1)B^0$$

$$+2M_N\xi(2\xi^2-1)\sqrt{\frac{\xi+1}{\xi-1}}C^0 + \frac{1-2\xi^2}{2(\xi-1)}E^0\Big], \tag{A6}$$

$$F_v^0 = \frac{1}{2\xi^2(1+\xi)}\Big[\xi A^0 - B^0 - 2M_N\xi\sqrt{\frac{\xi+1}{\xi-1}}C^0$$

$$+\frac{1}{2(\xi-1)}E^0\Big]. \tag{A7}$$

where $\xi = \sqrt{s}/2M_N$ is dimensionless Notice that the quantity D^0 does not enter in for the scalar and vector strengths. It is interesting to realize that inasmuch as the central potential dominates, it is really only the quantities A^0 and C^0 which are important. Indeed, if the differences between the scalar and vector nuclear densities are neglected, a relevant quantity which appears in the Dirac eikonal formalism is

$$-\frac{2M_N r F_s^0 + 2E_{lab} r F_v^0}{2ip_{lab}} = 4\pi A^0, \tag{A8}$$

That this should be true is not a surprise. A^0 is just the forward scattering amplitude, whose imaginary part is proportional to the total cross section.

3. Extracting Forward Amplitudes from Data

The problem is how to extract the NN parameters A^0, B^0, C^0, E^0 from the data. We do this in two ways. In the first way, we take some recent phase shift solutions to reconstruct the helicity amplitudes and then to use the above relations to get at the quantities we need. One must be very careful, however, since there exist many different parameterizations of the experimental phase shifts and of the scattering amplitude so that one must make sure that all of the parameterizations are consistent with one another. The second method involves a more direct determination of the relevant amplitudes from data.

a. Forward Amplitudes from $Q^2 = 1 - 6\,GeV^2$

Wallace has published [50] the Pauli amplitudes, A^0, B^0, C^0, D^0, E^0 for Hoshizaki's phase shift solutions up to $Q^2 = 4\,GeV^2$. In particular, Wallace uses [54] a more recent solution [58]

than that published in Refs. [55–57], as well as calculating at more energies. Therefore, we construct the optical potential strengths in this energy regime by using Eqs. (A6) and (A7) for Wallace's amplitudes.

At higher energies, we use the phase shift analysis of Higuchi and Hoshizaki [59] for pp phase shifts at $p_{lab} = 4\,GeV$, which translates to $Q^2 = 5.96\,GeV^2$, in order to reconstruct the T-matrix and extract the strengths as outlined. Using this method, we were able to construct the T-matrix and to reproduce the experimental data and theoretical predictions published by Hoshizaki [59]. This serves as a consistency check that we are using the phase shifts correctly.

We must stress the fact that at these energies the phase shifts are only loosely constrained, at best. Therefore, different phase shift analyses will yield different values for the optical potential strengths. However, our strengths are roughly consistent with those found in Ref. [48].

b. Forward Amplitudes at $Q^2 = 9.65$ and $20.86\,GeV^2$

Phase shift solutions provide a powerful method to summarize the scattering data and to predict observables at all momentum transfers. At higher energies, more and more partial waves become important (and the data becomes more and more scarce) and phase shift analyses become difficult. However, phase shift analyses do exist [60,61] for (lab) beam momenta of 6 GeV/c and 12 GeV/c; in quasi-elastic kinematics, these beam momenta translate to $Q^2 = 9.65$ and $20.86\,GeV^2$. However, the lack of constraining data as well as the idea that the high angular momentum partial waves are not negligible and must be modelled leads us away from the phase shifts. We will, however, take certain qualitative features from these analyses; see below. Further, the phase shift analyses do not emphasize the forward direction observables over the other angles. Indeed,

$$A^0 = \frac{\sigma}{8\pi}\left(1 - i\alpha_f\right), \tag{A9}$$

$$B^0 = \frac{\Delta\sigma_T}{-16\pi} - i\frac{F_2}{4k}, \tag{A10}$$

$$E^0 = \frac{\Delta\sigma_L}{-16\pi} + i\frac{F_3}{4k} - B^0, \tag{A11}$$

where α_f is the ratio of the real part to the imaginary part of the forward scattering amplitude and k is the center-of-mass momentum. The other real parts are $F_2 = \frac{p_{lab}}{k} \mathrm{Re}\, \phi_2(0°)$ and $F_3 = \frac{p_{lab}}{k} \mathrm{Re}\, [\phi_1(0°) - \phi_3(0°)]$. The longitudinal cross section, $\Delta\sigma_L$, is given by the difference of measured cross sections with beam and target proton spins aligned and anti-aligned with the beam direction with that of the both spins aligned along the beam direction. Similarly, the transverse cross section is measured by subtracting cross sections where the beam proton spin is aligned with the normal to the beam direction and the target spin is anti-aligned minus the cross section where both beam and target spins are aligned with the normal to the beam direction. The quantities F_2 and F_3 are evaluated using dispersion relations [83].

Thus, the only required quantity not available directly from the forward cross section data is the parameter C^0. However, this parameter can be obtained if enough data on the spin observables at small $-t$ is known. For instance, in the four component notation of Refs. [84–86], we can write two of the spin observables as

$$\frac{k^2}{\pi} \frac{d\sigma}{dt} P_n = \mathrm{Re}\, a^* e, \tag{A12}$$

$$\frac{k^2}{\pi} \frac{d\sigma}{dt} A_{00sk} = -\mathrm{Re}\, a^* d \sin\theta - \mathrm{Im}\, d^* e \cos\theta, \tag{A13}$$

where θ is the center-of-mass scattering angle and

$$A = \frac{a+b}{4ik}, \tag{A14}$$

$$B = \frac{a-b}{4ik}, \tag{A15}$$

$$C = -\frac{e}{4kq}, \tag{A16}$$

$$D = \frac{-a+b+c-d}{4ik}, \tag{A17}$$

$$E = \frac{-a+b+c+d}{4ikq^2}. \tag{A18}$$

Notice that both of these quantities, P_n and A_{sk} ($A_{sk} \equiv A_{00sk}$), vanish in the forward direction ($\theta = e = 0$). Their slopes (as a function of q, not $-t$) at $q = 0$, however, are finite. Taking the derivatives with respect to $q = |\mathbf{q}| = \sqrt{-t}$ and evaluating in the forward direction, we obtain

$$\frac{k^2}{\pi} \left(\frac{d\sigma}{dt}\right)_{t=0} \left(\frac{dP_n}{dq}\right)_{q=0} = \mathrm{Re}\, a^* \frac{e}{q}, \tag{A19}$$

$$\frac{k^2}{\pi} \left(\frac{d\sigma}{dt}\right)_{t=0} \left(\frac{dA_{sk}}{dq}\right)_{q=0} = -\frac{1}{k}\mathrm{Re}\, a^* d - \mathrm{Im}\, d^* \frac{e}{q}, \tag{A20}$$

where we have used $e/q \approx e'(q)$ in the forward direction. Note that e/q remains finite in this limit. We have also changed variables and written the differential cross section in Lorentz invariant form. Now, denoting x_R and x_I as the real and imaginary parts of the complex number x, we can use the above two equations to write

$$C_R = -\frac{a_I}{4k^2} - \frac{k}{4\pi} \frac{1}{a_R d_R + a_I d_I} \left(\frac{d\sigma}{dt}\right)_{t=0} \times$$
$$\left[d_R \left(\frac{dP_n}{dq}\right)_{q=0} + a_I \left(\frac{dA_{sk}}{dq}\right)_{q=0} \right], \tag{A21}$$

$$C_I = -\frac{a_R}{a_I} C_R - \frac{k}{4\pi a_I} \left(\frac{d\sigma}{dt}\right)_{t=0} \left(\frac{dP_n}{dq}\right)_{q=0}, \tag{A22}$$

where a superscript ^{0}, indicating the forward direction, is to be understood on the quantities $C_R, C_I, a_R, a_I, d_R, d_I$.

Thus, with these equations, and some good spin data, we can extract the optical potential strengths directly from data. We note that we have tested these equations for the spin parameter C on the $4\,GeV/c$ data of Hoshizaki [59] and they agree with the value calculated strictly by using phase shifts. This gives us confidence that these equations are reliable to use at higher energies.

The experimental values for the σ^{tot}, α_f, $\Delta\sigma_L$, $\Delta\sigma_T$, F_2 and F_3 are summarized in Refs. [60,61]. In order to complete the analysis described above, we need information on the slopes of P_n and A_{sk} at small q. In Refs. [87,88] the polarization P_n has been measured at $p_{lab} = 6\,GeV/c$. Better than that, an empirical fit to the data is given, which can be directly differentiated. By averaging these two values from the two references, we obtain the result

$$\left(\frac{dP_n}{dq}\right)_{q=0} = 0.494\,GeV^{-1} \quad \text{for} \quad \mathrm{p_{lab}} = 6\,GeV/c. \tag{A23}$$

The uncertainty in this quantity is only about 3%; see Refs. [87,88]. At $p_{lab} = 12\,GeV/c$, the polarization has been measured [89] and again an empirical fit is given. Thus, differentiating this quantity directly we find that

$$\left(\frac{dP_n}{dq}\right)_{q=0} = 0.215\,GeV^{-1} \quad \text{for} \quad \mathrm{p_{lab}} = 12\,GeV/c. \tag{A24}$$

To proceed, we now notice something amazing. Looking at the data for A_{sk} at $p_{lab} = 4\,GeV/c$ [59] we see that the experimental slope of A_{sk} is zero to a very good approximation. Indeed, explicit calculation based on Hoshizaki's phase shifts yield a slope of $0.014\,GeV^{-1}$. There is very little data for A_{sk} at higher energies, yet the phase shift solutions [60,61] also suggest that the slope of A_{sk} is very small. Based on this evidence, we assume that

$$\left(\frac{dA_{sk}}{dq}\right)_{q=0} = 0, \tag{A25}$$

at least for energies below $p_{lab} = 12\,GeV/c$.

Using the central values in the published data yields optical potential strengths which are larger in magnitude than the lower energy values. However, by adjusting the parameters within their experimental error bars, numbers in better agreement (more consistent) with the low energy data can be obtained. It is these numbers which are summarized in Table I. There is therefore considerable uncertainty in the last two rows of Table I. In particular, the forward scattering data we use to generate the strengths are displayed in Table IV. The intermediate Pauli amplitudes obtained in the manner described in this appendix are displayed in Table V.

Clearly, the most important of these parameters are A^0, which contains the information about the forward scattering amplitude, and the spin-flip parameter C^0 which is determined from the slopes of the forward spin observables.

APPENDIX B: DWBA AND CT EIKONAL WAVEFUNCTIONS

1. DWBA Eikonal Wavefunction

The expression for the DWBA wavefunction, Eq. (3.13), can be simplified by performing the spin algebra. First, we note that in the coordinate system (B, Z, ϕ), the cross product $\mathbf{B} \times \mathbf{p} = -Bp\check{\phi}$ ($B = |\mathbf{B}|$ and $p = |\mathbf{p}|$). To reduce the wavefunction to its fundamental dependence (linear) on the spin matrices, we define the quantities

$$\omega_1^{(+)}(\mathbf{B}, Z) = \int_{-\infty}^{Z} \frac{dZ'}{2ip} \Big[U_c(\mathbf{B}, Z')$$
$$-ipZ'\, U_{so}(\mathbf{B}, Z') \Big], \tag{B1}$$

$$\omega_2^{(+)}(\mathbf{B}, Z) = \frac{B}{2} \int_{-\infty}^{Z} dZ' \, U_{so}(\mathbf{B}, Z'). \tag{B2}$$

Then, we obtain the final DWBA wavefunction as

$$\Psi_{\mathbf{p}, -\check{\mathbf{s}}_R}^{(+)}(\mathbf{R}) = \mathcal{N} \begin{pmatrix} u_{\mathbf{p}}^{(+)}(\mathbf{R}) \\ w_{\mathbf{p}}^{(+)}(\mathbf{R}) \end{pmatrix} \chi_{-\check{\mathbf{s}}_R}, \tag{B3}$$

where

$$u_{\mathbf{p}}^{(+)} = e^{ipZ} e^{\omega_1^{(+)}} \left[\cos \omega_2^{(+)} + i\boldsymbol{\sigma} \cdot \check{\boldsymbol{\phi}} \sin \omega_2^{(+)} \right] \tag{B4}$$

$$w_{\mathbf{p}}^{(+)} = e^{ipZ} e^{\omega_1^{(+)}} \frac{-i}{E + M_N + V_s - V_v} \quad \times$$

$$\left\{ \boldsymbol{\sigma} \cdot \check{\mathbf{Z}} \left[\cos \omega_2^{(+)} \left(\omega_{1,Z}^{(+)} - \omega_{2,B}^{(+)} + ip \right) - \sin \omega_2^{(+)} \left(\omega_{1,B}^{(+)} + \omega_{2,Z}^{(+)} + \frac{1}{B} \right) \right] \right.$$

$$\left. + \boldsymbol{\sigma} \cdot \check{\mathbf{B}} \left[\sin \omega_2^{(+)} \left(\omega_{1,Z}^{(+)} - \omega_{2,B}^{(+)} + ip \right) + \cos \omega_2^{(+)} \left(\omega_{1,B}^{(+)} + \omega_{2,Z}^{(+)} \right) \right] \right\}, \tag{B5}$$

where

$$\omega_{i,Z} = \frac{\partial}{\partial Z} \omega_i, \tag{B6}$$

$$\omega_{i,B} = \frac{\partial}{\partial B} \omega_i, \tag{B7}$$

and where we have suppressed the argument $\mathbf{R}$ in ω_1, ω_2, V_s and V_v.

We note that the wavefunction for incoming boundary conditions is obtained simply by taking the complex conjugate of the potentials and changing the limits of integration. Thus, $\Psi_{\mathbf{p}, -\check{\mathbf{s}}_R}^{(-)}$ has the same form as Eqs. (B4) and (B5) except that $\omega_i^{(+)} \to \omega_i^{(-)}$, where $i = 1, 2$ and

$$\omega_1^{(-)}(\mathbf{B}, Z) = -\int_Z^{\infty} \frac{dZ'}{2ip} \left[U_c^*(\mathbf{B}, Z') + ipZ' \, U_{so}^*(\mathbf{B}, Z') \right], \tag{B8}$$

$$\omega_2^{(-)}(\mathbf{B}, Z) = -\frac{B}{2} \int_Z^{\infty} dZ' U_{so}^*(\mathbf{B}, Z'), \tag{B9}$$

where U^* represents the complex conjugate of the quantity U.

It is also instructive to consider the case where the optical potentials are small, in some sense. Then, we can perform an order by order expansion of the DWBA wavefunction, in terms of the potentials. This is useful as a practical matter because the size of the first-order

56

term of the DWBA is a good indicator of how accurate the OBO CT wavefunction will be, see Ref. [30]. Thus, we proceed by expanding in powers of ω_1 and neglecting terms of order $\mathcal{O}(\omega_i^3)$. We obtain,

$$\Psi^{(+)}_{\mathbf{p},-\check{\mathbf{s}}_R}(\mathbf{R}) = e^{ipZ} \sum_m \Psi^{(+)}_{m,\mathbf{p},-\check{\mathbf{s}}_R}(\mathbf{R}), \tag{B10}$$

where the subscript m indicates the order of the expansion of the potentials. Decomposing the wavefunction in terms of upper and lower components,

$$\Psi^{(+)}_{m,\mathbf{p},-\check{\mathbf{s}}_R}(\mathbf{R}) = \mathcal{N} \begin{pmatrix} u^{(+)}_{m,\mathbf{p}}(\mathbf{R}) \\ w^{(+)}_{m,\mathbf{p}}(\mathbf{R}) \end{pmatrix} \chi_{-\check{\mathbf{s}}_R}. \tag{B11}$$

We present explicit expressions for the order by order expansion of the DWBA wavefunction. We only need the first few terms.

$$u^{(+)}_{0,\mathbf{p}} = 1, \tag{B12}$$

$$w^{(+)}_{0,\mathbf{p}} = \frac{\boldsymbol{\sigma} \cdot \mathbf{p}}{E + M_N + V_s - V_v}, \tag{B13}$$

$$u^{(+)}_{1,\mathbf{p}} = \left(\omega^{(+)}_1 + i\omega^{(+)}_2 \boldsymbol{\sigma} \cdot \check{\boldsymbol{\phi}} \right), \tag{B14}$$

$$
\begin{aligned}
w^{(+)}_{1,\mathbf{p}} = {}& \frac{1}{E + M_N + V_s - V_v} \\
& \times \left\{ \boldsymbol{\sigma} \cdot \check{\mathbf{Z}} \left[p\omega^{(+)}_1 - i\omega^{(+)}_{1,Z} + i\omega^{(+)}_{2,B} + i\frac{\omega^{(+)}_2}{B} \right] \right. \\
& \left. + \boldsymbol{\sigma} \cdot \check{\mathbf{B}} \left[p\omega^{(+)}_2 - i\omega^{(+)}_{1,B} - i\omega^{(+)}_{2,Z} \right] \right\},
\end{aligned}
\tag{B15}
$$

$$u^{(+)}_{2,\mathbf{p}} = \left[\frac{1}{2} \left(\omega^{(+)}_1 \right)^2 - \frac{1}{2} \left(\omega^{(+)}_2 \right)^2 + i\boldsymbol{\sigma} \cdot \check{\boldsymbol{\phi}}\, \omega^{(+)}_1 \omega^{(+)}_2 \right], \tag{B16}$$

$$
\begin{aligned}
w^{(+)}_{2,\mathbf{p}} = {}& \frac{1}{E + M_N + V_s - V_v} \left\{ \boldsymbol{\sigma} \cdot \check{\mathbf{Z}} \left[\frac{p}{2} \left(\omega^{(+)}_1 \right)^2 - \frac{p}{2} \left(\omega^{(+)}_2 \right)^2 \right.\right. \\
& \left. - i\omega^{(+)}_1 \omega^{(+)}_{1,Z} + i\omega^{(+)}_2 \omega^{(+)}_{2,Z} + i\omega^{(+)}_1 \omega^{(+)}_{2,B} + i\omega^{(+)}_2 \omega^{(+)}_{1,B} + i\frac{\omega^{(+)}_1 \omega^{(+)}_2}{B} \right] \\
& + \boldsymbol{\sigma} \cdot \check{\mathbf{B}} \left[p\, \omega^{(+)}_1 \omega^{(+)}_2 - i\omega^{(+)}_1 \omega^{(+)}_{1,B} + i\omega^{(+)}_2 \omega^{(+)}_{2,B} \right.\\
& \left.\left. - i\omega^{(+)}_2 \omega^{(+)}_{1,Z} - i\omega^{(+)}_1 \omega^{(+)}_{2,Z} \right] \right\}.
\end{aligned}
\tag{B17}
$$

2. CT Eikonal Wavefunctions

Here, we show the explicit CT eikonal wavefunctions in our various approximation schemes. More notation is needed, so we introduce the quantity

$$\mathcal{U}_{cso}^{(2j)}(\mathbf{B}, Z, Z') = \mathcal{U}_c^{(2j)}(\mathbf{B}, Z, Z') - ipZ'\,\mathcal{U}_{so}^{(2j)}(\mathbf{B}, Z, Z'), \tag{B18}$$

where p/p_{2j} is set to unity. This CT potential (a number) with three arguments is not the operator $\widehat{\mathcal{U}}_{c(so)}$; although there is an intimate relationship. In fact,

$$\mathcal{U}_{c(so)}^{(2j)}(\mathbf{B}, Z, Z') = e^{i(p_{2m}-p)Z}\, e^{-i(p_{2j}-p)Z'}$$

$$\times \sum_{m=0}^{\infty} \langle 2m|\widehat{\mathcal{U}}_{c(so)}(\mathbf{B}, Z')|2j\rangle. \tag{B19}$$

In first-order calculations, a common simple quantity is the integral of these CT potentials which connect to the nucleon. Thus, we define the CT integrals as

$$\Omega_1^{(+)}(\mathbf{B}, Z) = \int_{-\infty}^{Z} \frac{dZ'}{2ip} \mathcal{U}_{cso}^{(0)}(\mathbf{B}, Z, Z'), \tag{B20}$$

$$\Omega_2^{(+)}(\mathbf{B}, Z) = \frac{B}{2} \int_{-\infty}^{Z} dZ'\, \mathcal{U}_{so}^{(0)}(\mathbf{B}, Z, Z'), \tag{B21}$$

and their derivatives as

$$\Omega_{i,Z}^{(+)}(\mathbf{R}) = \frac{\partial}{\partial Z}\Omega_i^{(+)}(\mathbf{R}), \tag{B22}$$

$$\Omega_{i,B}^{(+)}(\mathbf{R}) = \frac{\partial}{\partial B}\Omega_i^{(+)}(\mathbf{R}), \tag{B23}$$

where $i = 1, 2$.

a. Order By Order Wavefunction

The (outgoing) OBO wavefunction is defined such that

$$\Psi_{CT,\mathbf{p},-\check{\mathbf{s}}_R}^{(+)}(\mathbf{R}) = e^{ipZ} \sum_m \Psi_{m,\mathbf{p},-\check{\mathbf{s}}_R}^{OBO}(\mathbf{R}), \tag{B24}$$

where the index m indicates the order (0-2) of the expansion of the path ordered exponential. Using standard techniques and previously defined notation, the result is

$$\Psi_{m,\mathbf{p},-\check{\mathbf{s}}_R}^{OBO}(\mathbf{R}) = \mathcal{N} \begin{pmatrix} u_{m,\mathbf{p}}^{OBO}(\mathbf{R}) \\ w_{m,\mathbf{p}}^{OBO}(\mathbf{R}) \end{pmatrix} \chi_{-\check{\mathbf{s}}_R}. \tag{B25}$$

where

$$u_{0,\mathbf{p}}^{OBO} = 1 \tag{B26}$$

$$w_{0,\mathbf{p}}^{OBO} = \frac{\boldsymbol{\sigma} \cdot \mathbf{p}}{E + M_N}, \tag{B27}$$

$$u_{1,\mathbf{p}}^{OBO} = \left(\Omega_1 + i\Omega_2 \boldsymbol{\sigma} \cdot \check{\boldsymbol{\phi}} \right), \tag{B28}$$

$$w_{1,\mathbf{p}}^{OBO} = \left\{ \frac{\boldsymbol{\sigma} \cdot \check{\mathbf{Z}}}{E + M_N} \left[p\,\Omega_1 + i\frac{\Omega_2}{B} - i\Omega_{1,Z} + i\Omega_{2,B} \right] \right.$$
$$\left. + \frac{\boldsymbol{\sigma} \cdot \check{\mathbf{B}}}{E + M_N} \left[p\,\Omega_2 - i\Omega_{1,B} - i\Omega_{2,Z} \right] \right\}, \tag{B29}$$

$$u_{2,\mathbf{p}}^{OBO} = \left(\mathcal{A}_1 + i\mathcal{A}_2 \boldsymbol{\sigma} \cdot \check{\boldsymbol{\phi}} \right), \tag{B30}$$

$$w_{2,\mathbf{p}}^{OBO} = \left\{ \frac{\boldsymbol{\sigma} \cdot \check{\mathbf{Z}}}{E + M_N} \left[p\,\mathcal{A}_1 + i\frac{\mathcal{A}_2}{B} + -i\mathcal{A}_{1,Z} + i\mathcal{A}_{2,B} \right] \right.$$
$$\left. + \frac{\boldsymbol{\sigma} \cdot \check{\mathbf{B}}}{E + M_N} \left[p\,\mathcal{A}_2 - i\mathcal{A}_{1,B} - i\mathcal{A}_{2,Z} \right] \right\}, \tag{B31}$$

where we have defined two new (outgoing) "second-order functions" by

$$\mathcal{A}_1(\mathbf{B}, Z) = \int_{-\infty}^{Z} \frac{dZ'}{2ip} \int_{-\infty}^{Z'} \frac{dZ''}{2ip} \qquad \times$$
$$\left\{ \mathcal{U}_{cso}^{(0)}(Z, Z') U_{cso}^{(0,0)}(Z'') + B^2 p^2 \mathcal{U}_{so}^{(0)}(Z, Z') U_{so}^{(0,0)}(Z'') \right.$$
$$+ e^{i(p_2-p)(Z'-Z'')} \left(\mathcal{U}_{cso}^{(2)}(Z, Z') U_{cso}^{(2,0)}(Z'') + B^2 p^2 \mathcal{U}_{so}^{(2)}(Z, Z') U_{so}^{(2,0)}(Z'') \right)$$
$$\left. + e^{i(p_4-p)(Z'-Z'')} \mathcal{U}_{cso}^{(4)}(Z, Z') U_{cso}^{(4,0)}(Z'') \right\}, \tag{B32}$$

$$i\mathcal{A}_2(\mathbf{B}, Z) = -Bp \int_{\infty}^{Z} \frac{dZ'}{2ip} \int_{-\infty}^{Z'} \frac{dZ''}{2ip} \qquad \times$$
$$\left\{ \mathcal{U}_{cso}^{(0)}(Z, Z') U_{so}^{(0,0)}(Z'') + \mathcal{U}_{so}^{(0)}(Z, Z') U_{cso}^{(0,0)}(Z'') \right.$$
$$+ e^{i(p_2-p)(Z'-Z'')} \left(\mathcal{U}_{cso}^{(2)}(Z, Z') U_{so}^{(2,0)}(Z'') + \mathcal{U}_{so}^{(2)}(Z, Z') U_{cso}^{(2,0)}(Z'') \right)$$
$$\left. + e^{i(p_4-p)(Z'-Z'')} \mathcal{U}_{so}^{(4)}(Z, Z') U_{cso}^{(4,0)}(Z'') \right\}, \tag{B33}$$

and we have suppressed the impact parameter inside the arguments of the CT functions for clarity.

There are a few analytic checks of these expressions. First, in the CT limit, when $p_4 \approx p_2 \approx p$ becomes very large, then $\Omega_{1(2)}$ and $\mathcal{A}_{1(2)}$ approach zero and CT is obtained. The next thing to notice is that the OBO_1 wavefunction has the same form as the $DWBA_1$ with the simple substitution $\omega \to \Omega$. Thus, at low energies (below excited state threshhold), p_2 and p_4 are purely imaginary so that $\mathcal{U}_{c(so)}^{(0)} \to U_{c(so)}^{(0,0)}$. Thus, insofar as we can take $U_{c(so)}^{(0,0)} = U_{c(so)}$, see Eqs. (4.11) and (4.12), we see that $\Omega \to \omega$ and the $DWBA_1$ is obtained, modulo, of course, the small CTD effects described above. The same analysis works with the second-order calculation. In particular, below threshold, the exponentials damp most of the terms so that the only ones which contribute are $\mathcal{U}_{cso(so)}^{(0)} \to U_{cso(so)}^{(0,0)}$. Thus, in this low energy limit, $\mathcal{A}_1 \to \omega_1^2/2 - \omega_2^2/2$ and $\mathcal{A}_2 \to \omega_1 \omega_2$. Some simple algebra then yields the desired result that, in the low energy limit, the OBO wavefunction approaches the $DWBA$.

b. Exponential Approximation Wavefunction

In this approximation, the CT wavefunction is obtained by taking the first order result and exponentiating. Thus, the EA has the same relationship to the OBO_1 as does the $DWBA$ to the $DWBA_1$. This is equivalent to neglecting the path ordering. Then the (outgoing) EA wavefunction can be written down immediately:

$$\Psi_{CT,\mathbf{p},-\check{s}_R}^{(+)}(\mathbf{R}) \approx \Psi_{\mathbf{p},-\check{s}_R}^{EA}(\mathbf{R}), \tag{B34}$$

where

$$\Psi_{\mathbf{p},-\check{s}_R}^{EA}(\mathbf{R}) = \mathcal{N} \begin{pmatrix} u_{\mathbf{p}}^{EA}(\mathbf{R}) \\ w_{\mathbf{p}}^{EA}(\mathbf{R}) \end{pmatrix} \chi_{-\check{s}_R}, \tag{B35}$$

and

$$u_{\mathbf{p}}^{EA} = e^{ipZ} e^{\Omega_1} \left[\cos \Omega_2 + i\boldsymbol{\sigma} \cdot \check{\boldsymbol{\phi}} \sin \Omega_2 \right], \tag{B36}$$

$$
\begin{aligned}
w_{\mathbf{p}}^{EA} = \frac{-i e^{ipZ} e^{\Omega_1}}{E + M_N} \Big\{ &\boldsymbol{\sigma} \cdot \check{\mathbf{Z}} \Big[\cos \Omega_2 \left(\Omega_{1,Z} - \Omega_{2,B} + ip \right) \\
&- \sin \Omega_2 \left(\Omega_{1,B} + \Omega_{2,Z} - \frac{1}{B} \right) \Big] \\
&+ \boldsymbol{\sigma} \cdot \check{\mathbf{B}} \Big[\sin \Omega_2 \left(\Omega_{1,Z} - \Omega_{2,B} + ip \right) \\
&+ \cos \Omega_2 \left(\Omega_{1,B} + \Omega_{2,Z} \right) \Big] \Big\}.
\end{aligned}
\tag{B37}
$$

We again explore the high- and low-energy limits to perform a check on this wavefunction. At very high energies, $\Omega_{1(2)}$ become very small and approach zero. When this happens, it is easy to see that CT is obtained. At very low energies, aside from small quadratic CTD effects, the EA approaches the $DWBA$.

<div align="center">c. Low Energy Wavefunction</div>

The CT wavefunction in the LEE approximation is defined so that the expectation value of the CT operators in the nucleon is separated out and the rest is treated in perturbation theory. In Ref. [30] we defined the LEE approximation so that the wavefunction reduced to the $DWBA$ in the zero'th order. Due to quadratic and CTD effects, this will no longer be exactly true. It is necessary to define more notation to obtain the (outgoing) LEE wavefunction. Thus we define :

$$\omega_{01}(\mathbf{B}, Z) \equiv \int_{-\infty}^{Z} \frac{dZ'}{2ip} \Big[U_c^{(0,0)}(\mathbf{B}, Z')$$

$$-ipZ'U_{so}^{(0,0)}(\mathbf{B}, Z') \Big], \tag{B38}$$

$$\omega_{02}(\mathbf{B}, Z) \equiv \frac{B}{2} \int_{-\infty}^{Z} dZ'U_{so}^{(0,0)}(\mathbf{B}, Z'), \tag{B39}$$

along with the reduced CT integrals

$$\Omega_{01(2)}(\mathbf{B}, Z) = \Omega_{1(2)}(\mathbf{B}, Z) - \omega_{01(2)}(\mathbf{B}, Z). \tag{B40}$$

With these preliminaries we obtain the (outgoing) LEE wavefunction as

$$\Psi_{CT,\mathbf{p},-\check{\mathbf{s}}_R}^{(+)}(\mathbf{R}) = e^{ipZ} \sum_m \Psi_{m,\mathbf{p},-\check{\mathbf{s}}_R}^{LEE}(\mathbf{R}), \tag{B41}$$

where the index m indicates the order of the expansion of the perturbation; $m = 0$ or 1. The result is

$$\Psi_{m,\mathbf{p},-\check{\mathbf{s}}_R}^{LEE}(\mathbf{R}) = \mathcal{N} \begin{pmatrix} u_{m,\mathbf{p}}^{LEE}(\mathbf{R}) \\ w_{m,\mathbf{p}}^{LEE}(\mathbf{R}) \end{pmatrix} \chi_{-\check{\mathbf{s}}_R}, \tag{B42}$$

where

<div align="center">61</div>

$$u_{0,\mathbf{p}}^{LEE} = e^{\omega_{01}} \left[\cos\omega_{02} + i\boldsymbol{\sigma} \cdot \check{\boldsymbol{\phi}} \sin\omega_{02} \right], \tag{B43}$$

$$w_{0,\mathbf{p}}^{LEE} = \frac{e^{\omega_{01}}}{E + M_N} \qquad \times \qquad \left\{ \vphantom{\frac{i}{B}} \right.$$

$$\boldsymbol{\sigma} \cdot \check{\mathbf{Z}} \cos\omega_{02} \left(p - i\omega_{01,Z} + i\omega_{02,B} \right)$$

$$\boldsymbol{\sigma} \cdot \check{\mathbf{Z}} \sin\omega_{02} \left(i\omega_{01,B} + i\omega_{02,Z} + \frac{i}{B} \right)$$

$$\boldsymbol{\sigma} \cdot \check{\mathbf{B}} \cos\omega_{02} \left(-i\omega_{01,B} - i\omega_{02,Z} \right)$$

$$\left. \boldsymbol{\sigma} \cdot \check{\mathbf{B}} \sin\omega_{02} \left(p - i\omega_{01,Z} + i\omega_{02,B} \right) \right\}, \tag{B44}$$

$$u_{1,\mathbf{p}}^{LEE} = e^{\omega_{01}} \Big[\left(\cos\omega_{02} + i\boldsymbol{\sigma} \cdot \check{\boldsymbol{\phi}} \sin\omega_{02} \right) \Omega_{01} +$$

$$\left(-\sin\omega_{02} + i\boldsymbol{\sigma} \cdot \check{\boldsymbol{\phi}} \cos\omega_{02} \right) \Omega_{02} \Big], \tag{B45}$$

$$w_{1,\mathbf{p}}^{LEE} = \frac{e^{\omega_{01}}}{E + M_N} \qquad \times \qquad \left\{ \vphantom{\frac{1}{B}} \right.$$

$$\boldsymbol{\sigma} \cdot \check{\mathbf{Z}} \cos\omega_{02} [\left(p - i\omega_{01,Z} + i\omega_{02,B} \right) \Omega_{01} +$$

$$i \left(\omega_{01,B} + \omega_{02,Z} + \frac{1}{B} \right) \Omega_{02} - i\Omega_{01,Z} + i\Omega_{02,B}]$$

$$\boldsymbol{\sigma} \cdot \check{\mathbf{Z}} \sin\omega_{02} [\left(-p + i\omega_{01,Z} - i\omega_{02,B} \right) \Omega_{02} +$$

$$i \left(\omega_{01,B} + \omega_{02,Z} + \frac{1}{B} \right) \Omega_{01} + i\Omega_{01,B} + i\Omega_{02,Z}]$$

$$\boldsymbol{\sigma} \cdot \check{\mathbf{B}} \cos\omega_{02} [\left(p - i\omega_{01,Z} + i\omega_{02,B} \right) \Omega_{02} -$$

$$i \left(\omega_{01,B} + \omega_{02,Z} \right) \Omega_{01} - i\Omega_{01,B} - i\Omega_{02,Z}]$$

$$\boldsymbol{\sigma} \cdot \check{\mathbf{B}} \sin\omega_{02} [\left(p - i\omega_{01,Z} + i\omega_{02,B} \right) \Omega_{01} +$$

$$\left. i \left(\omega_{01,B} + \omega_{02,Z} \right) \Omega_{02} - i\Omega_{01,Z} + i\Omega_{02,B}] \right\}, \tag{B46}$$

$$u_{2,\mathbf{p}}^{LEE} = e^{\omega_{01}} \Big[\left(\cos\omega_{02} + i\boldsymbol{\sigma} \cdot \check{\boldsymbol{\phi}} \sin\omega_{02} \right) \mathcal{B}_1 +$$

$$\left(-\sin\omega_{02} + i\boldsymbol{\sigma} \cdot \check{\boldsymbol{\phi}} \cos\omega_{02} \right) \mathcal{B}_2 \Big], \tag{B47}$$

$$w_{2,\mathbf{p}}^{LEE} = \frac{e^{\omega_{01}}}{E + M_N} \qquad \times \qquad \Bigg\{$$

$$\boldsymbol{\sigma} \cdot \check{\mathbf{Z}} \cos \omega_{02} \Big[\big(p - i\omega_{01,Z} + i\omega_{02,B}\big) \mathcal{B}_1 +$$

$$i\left(\omega_{01,B} + \omega_{02,Z} + \frac{1}{B}\right)\mathcal{B}_2 - i\mathcal{B}_{1,Z} + i\mathcal{B}_{2,B}\Big]$$

$$\boldsymbol{\sigma} \cdot \check{\mathbf{Z}} \sin \omega_{02} \Big[\big(-p + i\omega_{01,Z} - i\omega_{02,B}\big)\mathcal{B}_2 +$$

$$i\left(\omega_{01,B} + \omega_{02,Z} + \frac{1}{B}\right)\mathcal{B}_1 + i\mathcal{B}_{1,B} + i\mathcal{B}_{2,Z}\Big]$$

$$\boldsymbol{\sigma} \cdot \check{\mathbf{B}} \cos \omega_{02} \Big[\big(p - i\omega_{01,Z} + i\omega_{02,B}\big)\mathcal{B}_2 -$$

$$i\left(\omega_{01,B} + \omega_{02,Z}\right)\mathcal{B}_1 - i\mathcal{B}_{1,B} - i\mathcal{B}_{2,Z}\Big]$$

$$\boldsymbol{\sigma} \cdot \check{\mathbf{B}} \sin \omega_{02} \Big[\big(p - i\omega_{01,Z} + i\omega_{02,B}\big)\mathcal{B}_1 +$$

$$i\left(\omega_{01,B} + \omega_{02,Z}\right)\mathcal{B}_2 - i\mathcal{B}_{1,Z} + i\mathcal{B}_{2,B}\Big]\Bigg\}, \tag{B48}$$

where we have defined two new functions, in analogy to $\mathcal{A}_{1(2)}$, to be

$$\mathcal{B}_1(\mathbf{B}, Z) = \int_{-\infty}^{Z} \frac{dZ'}{2ip} \int_{-\infty}^{Z'} \frac{dZ''}{2ip} \Bigg\{ e^{i(p_2 - p)(Z' - Z'')\, (0,0)} \mathcal{U}_{cso}^{(2)}(Z, Z') U_{cso}^{(2,0)}(Z'')$$

$$+ B^2 p^2 e^{i(p_2 - p)(Z' - Z'')\, (0,0)} \mathcal{U}_{so}^{(2)}(Z, Z') U_{so}^{(2,0)}(Z'')$$

$$+ e^{i(p_4 - p)(Z' - Z'')\, (0,0)} \mathcal{U}_{cso}^{(4)}(Z, Z') U_{cso}^{(4,0)}(Z'') \Bigg\}, \tag{B49}$$

$$i\mathcal{B}_2(\mathbf{B}, Z) = -Bp \int_{-\infty}^{Z} \frac{dZ'}{2ip} \int_{-\infty}^{Z'} \frac{dZ''}{2ip} \Bigg\{ e^{i(p_2 - p)(Z' - Z'')\, (0,0)} \mathcal{U}_{so}^{(2)}(Z, Z') U_{cso}^{(2,0)}(Z'')$$

$$+ e^{i(p_2 - p)(Z' - Z'')\, (0,0)} \mathcal{U}_{cso}^{(2)}(Z, Z') U_{so}^{(2,0)}(Z'')$$

$$+ e^{i(p_4 - p)(Z' - Z'')\, (0,0)} \mathcal{U}_{so}^{(4)}(Z, Z') U_{cso}^{(4,0)}(Z'') \Bigg\}. \tag{B50}$$

We have also defined the new functions

$$^{(0,0)}\mathcal{U}_{cso(so)}^{(2j)}(Z, Z') = \mathcal{U}_{cso(so)}(Z, Z')$$

$$- e^{i(p_{2j} - p)(Z - Z')} U_{cso(so)}^{(0,0)}(Z'). \tag{B51}$$

The behavior of this LEE wavefunction at low energies has already been briefly discussed. Note that at very low energies, $\Omega_{0i} \to 0$ as well as $^{(0,0)}\mathcal{U}_{cso(so)} \to 0$. Therefore, except for quadratic and CTD effects, the LEE wavefunction approaches the $DWBA$ wavefunction for low energies. One can also check this wavefunction at high energies where the potentials $\Omega_{0i} \to -\omega_{0i}$. Now, this wavefunction claims to be correct only to second order in the CT potentials. Thus, if we make the replacement that $\Omega_{0i} \to -\omega_{0i}$, we can expand the resulting

wavefunction to first order in the potentials ω_{0i}. Then, in addition, letting $\cos\omega_{02} \to 1 - \omega_{02}^2/2$, $\sin\omega_{02} \to \omega_{02}$ and $e^{\omega_{01}} \to 1 + \omega_{01} + \omega_{01}^2/2$ it is relatively simple to show that, to within terms of $\mathcal{O}(\omega_0{}^3)$, the LEE_1 wavefunction approaches the plane wave result for very large momenta. In case the reader wishes to verify the above statement, an intermediate result is that, in this limit, the $\mathcal{B}_1 = \left(\omega_{01}^2 - \omega_{02}^2\right)/2 + \mathcal{O}(\omega_0^3)$ and $\mathcal{B}_2 = \omega_{01}\,\omega_{02} + \mathcal{O}(\omega_0^3)$.
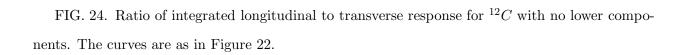
FIGURES

FIG. 1. Schematic drawing of $(\vec{e}, e'\vec{p})$ reaction.

FIG. 2. Coordinate system used to describe the $(\vec{e}, e'\vec{N})$ reaction.

FIG. 3. The second-order cross section ratios; $M_2 = 1.44\,GeV$.

FIG. 4. The second-order cross section ratios; $M_2 = 1.80\,GeV$.

FIG. 5. Total cross section ratios for ^{12}C. Solid (circles) is DWBA, dotdashed (diamonds) includes CT, via EA, for $M_2 = 1.44\,GeV$, dashed (boxes) have $M_2 = 1.80\,GeV$.

FIG. 6. Total cross section ratios for ^{40}Ca. The curves are as in Figure 5.

FIG. 7. Total cross section ratios for ^{208}Pb. The curves are as in Figure 5.

FIG. 8. Ratio of integrated longitudinal to transverse response for ^{12}C. Dotted (fancy boxes) is plane wave result, solid (circles) is DWBA, dotdashed (diamonds) and dashes (boxes) are CT-included cases for light and heavy excited state masses.

FIG. 9. Ratio of integrated longitudinal to transverse response for ^{40}Ca. The curves are as in Figure 8.

FIG. 10. Ratio of integrated longitudinal to transverse response for ^{208}Pb. The curves are as in Figure 8.

FIG. 11. Current conservation violations for ^{12}C. The curves are as in Figure 8.

FIG. 12. Current conservation violations for ^{40}Ca. The curves are as in Figure 8.

FIG. 13. Current conservation violations for ^{208}Pb. The curves are as in Figure 8.

FIG. 14. Differential unpolarized cross section and normal polarization for ^{12}C at $Q^2 = 0.96\,GeV^2$. The curves are as in Figure 8.

FIG. 15. Differential unpolarized cross section and normal polarization for ^{12}C at $Q^2 = 20.86\,GeV^2$. The curves are as in Figure 8.

FIG. 16. Effect of different electron kinematics at $Q^2 = 5.96\,GeV^2$. The dotdashed curve is the EA for $M_2 = 1.44\,GeV$, the dashed curve is the OBO_1, the dotted curve is the LEE_1. The solid curves are the $DWBA$ and the plane wave result, the context identifies them.

FIG. 17. Differential unpolarized response functions for ^{208}Pb at $Q^2 = 3.25\,GeV^2$. The curves are as in Figure 8.

FIG. 18. Differential normal response functions for ^{208}Pb at $Q^2 = 3.25\,GeV^2$. The curves are as in Figure 8.

FIG. 19. Cross section ratios for finite-sized wavepacket.

FIG. 20. Current conservation violations for finite-sized wavepacket.

FIG. 21. Effect of Fermi motion.

FIG. 22. Total cross section ratio for ^{12}C with no lower components. The upper CT curve and the lower DWBA curve are calculated with wavefunctions having no lower components. The point is that the ratio is independent of the lower components.

FIG. 23. Current conservation violations for ^{12}C with no lower components. In this figure, the dotted curve is the Born calculation with no lower components; the other curves are as in Figure 22.

FIG. 24. Ratio of integrated longitudinal to transverse response for ^{12}C with no lower components. The curves are as in Figure 22.

TABLES

TABLE I.   Energy dependent strengths of optical potentials. Q^2 is in GeV^2 and p_{lab} is in GeV. $r = -4\pi i p_{lab}/M_N$.

Q^2	p_{lab}	$r\, F_s^0(fm^2)$	$r\, F_v^0(fm^2)$	$\rho_0\, r\, F_s^0(MeV)$	$\rho_0\, r\, F_v^0(MeV)$
0.96	1.1	$-9.566 + 1.768\,i$	$5.720 - 2.291\,i$	$-313.3 + 57.91\,i$	$187.4 - 75.05\,i$
1.88	1.7	$-9.550 + 3.748\,i$	$4.970 - 3.895\,i$	$-312.8 + 122.8\,i$	$162.8 - 127.6\,i$
2.38	2.0	$-10.46 + 4.219\,i$	$4.912 - 3.936\,i$	$-342.6 + 138.2\,i$	$160.9 - 128.9\,i$
3.25	2.5	$-7.243 + 4.047\,i$	$3.396 - 3.573\,i$	$-237.3 + 132.6\,i$	$111.2 - 117.0\,i$
4.14	3.0	$-10.75 + 6.735\,i$	$3.836 - 4.124\,i$	$-352.0 + 220.6\,i$	$125.6 - 135.1\,i$
5.96	4.0	$-7.091 + 2.147\,i$	$2.155 - 2.540\,i$	$-232.3 + 70.33\,i$	$70.59 - 83.20\,i$
9.65	6.0	$-7.681 + 2.398\,i$	$1.831 - 2.380\,i$	$-251.6 + 78.56\,i$	$59.98 - 77.96\,i$
20.86	12.0	$-7.631 + 10.73\,i$	$1.168 - 2.809\,i$	$-250.0 + 351.4\,i$	$38.27 - 92.03\,i$

TABLE II.   Cross section and ratio of real to imaginary parts of forward scattering amplitude, as given by optical potential strengths.

Q^2 (GeV^2)	E_{lab} (GeV)	σ (mb)	α_f (unitless)
0.96	1.45	30.1	0.43
1.88	1.94	47.7	-0.17
2.38	2.21	47.5	-0.22
3.25	2.67	46.0	-0.40
4.14	3.14	44.3	-0.30
5.96	4.11	42.2	-0.26
9.65	6.07	40.8	-0.32
20.86	12.04	39.6	-0.29

TABLE III. Calculational kinematics.

Q^2	E_i	θ_e	$\left(\frac{d\sigma}{d\Omega_{k'}}\right)_{Mott}$	V_L	V_T	V_{TT}	V_{LT}
(GeV^2)	(GeV)	(deg)	(nb)				
0.96	4.0	15.1	1091.	0.62	0.41	0.39	-0.70
1.88	4.0	22.8	203.0	0.43	0.37	0.33	-0.54
2.38	4.0	27.0	103.6	0.36	0.36	0.30	-0.48
3.25	4.0	34.8	36.90	0.27	0.36	0.26	-0.41
4.14	4.0	44.6	13.40	0.21	0.40	0.23	-0.36
5.96	4.0	84.5	0.8865	0.14	1.01	0.19	-0.41
5.96	6.0	34.5	17.07	0.14	0.28	0.19	-0.25
5.96	11.0	22.7	140.7	0.14	0.20	0.19	-0.24
9.65	15.0	14.7	85.35	0.072	0.15	0.13	-0.14
20.86	21.0	18.2	18.24	0.021	0.098	0.072	-0.060

TABLE IV. Forward scattering data at $p_{lab} = 6$ and $12\,GeV/c$.

		$p_{lab} = 6\,GeV/c$			
σ^{tot}	$=$	$40.75\,mb$	α_f	$=$	-0.32
$\Delta\sigma_T$	$=$	$0.35\,mb$	F_2	$=$	$-4.60\,GeV^{-1}$
$\Delta\sigma_L$	$=$	$-1.04\,mb$	F_3	$=$	$4.60\,GeV^{-1}$
$\left(\frac{d\sigma}{dt}\right)_{t=0}$	$=$	$93.0\,mb$	$\left(\frac{dP_n}{dq}\right)_{q=0}$	$=$	$0.494\,GeV^{-1}$
		$p_{lab} = 12\,GeV/c$			
σ^{tot}	$=$	$39.60\,mb$	α_f	$=$	-0.29
$\Delta\sigma_T$	$=$	$0.01\,mb$	F_2	$=$	$-6.05\,GeV^{-1}$
$\Delta\sigma_L$	$=$	$-0.73\,mb$	F_3	$=$	$3.55\,GeV^{-1}$
$\left(\frac{d\sigma}{dt}\right)_{t=0}$	$=$	$65.0\,mb$	$\left(\frac{dP_n}{dq}\right)_{q=0}$	$=$	$0.215\,GeV^{-1}$

TABLE V. Pauli amplitudes for pp scattering

Q^2	A^0	B^0	C^0	E^0
(GeV^2)	(GeV^{-2})	(GeV^{-2})	(GeV^{-3})	(GeV^{-2})
0.96	$3.08 - 1.31\,i$	$-0.22 + 1.21\,i$	$-1.76 - 6.55\,i$	$0.69 + 0.02\,i$
1.88	$4.87 + 0.81\,i$	$-0.23 + 1.03\,i$	$-3.13 - 5.44\,i$	$0.82 - 0.05\,i$
2.38	$4.85 + 1.06\,i$	$-0.38 + 0.71\,i$	$-3.11 - 5.22\,i$	$0.81 + 0.16\,i$
3.25	$4.70 + 1.86\,i$	$-0.14 + 0.48\,i$	$-2.81 - 3.35\,i$	$0.29 + 0.16\,i$
4.14	$4.53 + 1.34\,i$	$-0.05 + 0.47\,i$	$-3.41 - 3.95\,i$	$0.15 - 0.01\,i$
5.96	$4.31 + 1.13\,i$	$-0.04 + 0.40\,i$	$-1.62 - 2.13\,i$	$0.12 - 0.09\,i$
9.65	$4.16 + 1.33\,i$	$-0.02 + 0.19\,i$	$-1.34 - 1.62\,i$	$0.07 - 0.00\,i$
20.86	$4.05 + 1.17\,i$	$-0.00 + 0.13\,i$	$-1.61 - 0.87\,i$	$0.04 - 0.05\,i$